

Report No. AEA-RS-1231

BENCHMARK TESTING OF JEF2.2 DATA
FOR SHIELDING APPLICATIONS :
ANALYSIS OF THE WINFRITH IRON 88
BENCHMARK EXPERIMENT

G.A.Wright and M.J.Grimstone

Reactor Physics, Shielding and Criticality Department
Safety Engineering Systems Division
AEA Reactor Services
Winfrith Technology Centre,
Dorchester, Dorset. DT2 8DH

March 1993

14090463

**BENCHMARK TESTING OF JEF2.2 DATA
FOR SHIELDING APPLICATIONS :**

**ANALYSIS OF THE WINFRITH IRON 88
BENCHMARK EXPERIMENT**

G.A.Wright and M.J.Grimstone

AEA Project Reference No. ND1

NSRMU Project Reference No. RPS/AGR/05

SUMMARY

The JEF2.2 nuclear data library has recently been released for benchmark testing. One application of the data will be in deep penetration shielding calculations in which the important governing physical processes are different from those encountered in criticality or core physics calculations. Thus a separate shielding benchmarking programme is required to validate the data for these applications. The shielding benchmarking in the U.K. comprises two stages, involving analysis firstly of single material experiments and secondly of experiments consisting of simple representations of practical shield configurations with several materials. This analysis is carried out using the Monte Carlo code MCBEND. One of the single material benchmarks which has been analysed is the Iron 88 Benchmark Experiment performed at Winfrith in the U.K. The results show that the JEF2.2 data produce results which are an improvement over those obtained using UKNDL data. There is still, however, the possibility of a deficiency in the Fe56 data in the 0.58 MeV to 1.35 MeV region. Various methods of evaluating the group-averaged Fe56 cross-section have been used in this work, the results showing that the energy group scheme (1/128 lethargy width) in which the data is held in the Fe56 resonance region is not fine enough to eliminate all dependence on resonance shielding. Totally shielded data and data derived using a simple subgroup method gave results which were in much better agreement with experiment than those obtained using infinite dilution Fe56 cross-sections.

Reactor Physics, Shielding and Criticality Department
Safety Engineering Systems Division
AEA Reactor Services

March 1993

14090464

CONTENTS

SUMMARY	
1.	INTRODUCTION 1
2.	DESCRIPTION OF THE EXPERIMENT 1
2.1	The ASPIS shielding facility
2.2	The iron 88 benchmark experimental array
2.3	Activation detector measurements in the iron 88 benchmark
2.4	Source description
3.	DESCRIPTION OF THE MCBEND CALCULATIONS 3
3.1	Geometry modelling
3.2	Source modelling
3.3	Material modelling
3.4	Variance reduction
3.5	Nuclear data
3.6	Detector cross-sections
3.7	Details of the MCBEND runs
4.	DISCUSSION OF THE RESULTS 6
4.1	S32(n,p)P32 detector
4.2	In115(n,n')In115m detector
4.3	Rh103(n,n')Rh103m detector
4.4	Au197(n, γ)Au198/Cd detector
4.5	Al27(n, α)Na24 detector
4.6	Discussion of calculation uncertainties
4.7	Comparison of the different methods of evaluating the group-averaged Fe56 cross-section
4.8	Assessment of the JEF2.2 data
5.	CONCLUSIONS 10
	REFERENCES 11

FIGURES

1. Schematic side elevation of the iron 88 single material benchmark experiment
2. Measurement locations for the iron 88 single material benchmark experiment
3. Schematic diagram of fission plate
4. Diagram of fuel element
5. Disposition of fuel in fission plate
6. Predicted and measured $S32(n,p)P32$ reaction rates along central axis
7. Predicted and measured $In115(n,n')In115m$ reaction rates along central axis
8. Predicted and measured $Rh103(n,n')Rh103m$ reaction rates along central axis
9. Predicted and measured $Au197(n,\gamma)Au198/Cd$ reaction rates along central axis
10. Predicted and measured $Al27(n,\alpha)Na24$ reaction rates along central axis
11. C/M values for $S32(n,p)P32$ detector along central axis
12. C/M values for $In115(n,n')In115m$ detector along central axis
13. C/M values for $Rh103(n,n')Rh103m$ detector along central axis
14. C/M values for $Au197(n,\gamma)Au198/Cd$ detector along central axis
15. C/M values for $Al27(n,\alpha)Na24$ detector along central axis
16. Sensitivity of the $S32(n,p)P32$ reaction rate after 67 cm of mild steel to the Fe56 cross-sections.
17. Sensitivity of the $In115(n,n')In115m$ reaction rate after 67 cm of mild steel to the Fe56 cross-sections.
18. Sensitivity of the $Rh103(n,n')Rh103m$ reaction rate after 67 cm of mild steel to the Fe56 cross-sections.

1. INTRODUCTION

The JEF2 nuclear data library [1] has now been released in the form of JEF2.2 for benchmark testing [2]. For shielding applications the benchmarking in the U.K. is being done in two stages. The first stage involves the analysis of single material benchmark experiments by the Monte Carlo code MCBEND [3] whilst the second stage will extend the analysis to experiments consisting of simple representations of practical shield configurations with several materials. During 1992/93 two such single material experiments have been analysed using JEF2 data : an iron benchmark and a water benchmark. The iron benchmark experiment was performed in 1988 and is thus known as the Iron 88 Benchmark Experiment. This report describes the analysis of the iron experiment ; a separate report [4] describes that of the water benchmark.

Section 2 of this report describes the iron benchmark experiment, section 3 describes the MCBEND calculation whilst section 4 describes and discusses the results. Finally section 5 draws some conclusions from this work.

2. DESCRIPTION OF THE EXPERIMENT

2.1 The ASPIS Shielding Facility

The ASPIS shielding facility is installed on the NESTOR reactor at Winfrith. NESTOR is a light water cooled, graphite and light water moderated reactor which operates at powers of up to 30 kW and is used as a source of neutrons for a wide range of applications. The core of the reactor, which comprises 26 MTR (Materials Test Reactor) type fuel elements, is contained within an annulus formed by two concentric aluminium vessels through which water circulates. The inner vessel is filled with graphite to form an inner reflector. The outer tank is surrounded by an external graphite reflector in the form of a block having dimensions 182 cm x 182 cm x 122 cm which contains the control plate slots adjacent to the vessel wall. Leading off each of the four faces of the external reflector is an experiment cave which can be isolated from the reactor by shutters composed of boral or combinations of neutron/gamma-ray shield materials.

ASPIS is located in the NESTOR cave C. Shield components, which are in the main slabs or tanks, are mounted vertically in a mobile tank which has an internal cross-sectional area of 1.8 m x 1.9 m and a length of 3.7 m. A fission plate is located within the experimental shield array. The loaded tank is moved into the cave where thermal neutrons leaking from the outer graphite reflector of NESTOR are used to drive the fission plate to provide a well defined neutron source for penetration measurements. The fission plate is manufactured from 93% enriched uranium/aluminium alloy and approximates to a disc source with an effective radius of 56 cm and a thickness of 2 mm. The absolute source strength is determined by fission product counting and the spatial distribution via detailed low energy flux mapping with activation detectors.

The neutron flux levels within an ASPIS shield contain contributions from sources in the fission plate and from the NESTOR core and it is essential that the NESTOR contribution is subtracted from all measured responses to arrive at the response resulting from the fission plate sources.

2.2 The Iron 88 Benchmark experimental array

The Iron 88 Benchmark experimental array irradiated in the ASPIS shielding facility is shown schematically in side elevation in Figure 1. The array comprises three regions; the source region containing moderator and the fission plate, the shield made from 13 mild steel plates, each of approximately 5.1 cm thickness, and a deep backing shield manufactured from mild and stainless steel. To allow detector access within the shield 6 mm spacers are placed between each slab component. In practice the depth of the air gaps varies owing to positional uncertainties of the plates and their flatness. The 6 mm gap is therefore nominal and an average gap of 7.4 mm was measured for the experiment. The axial dimensions of the experimental components are given in Table 1. The outer boundaries of the experimental region are formed by the walls and floor of the ASPIS trolley and by the roof of the ASPIS cave. The floor and walls of the trolley are manufactured from 1.91 cm

loading within each element has been arranged to the specification shown in Figure 5 by the substitution of aluminium blanks where necessary.

The approach taken to obtain the absolute power distribution within the fission plate is summarised as follows:

- (1) $\text{Mn55}(n,\gamma)\text{Mn56}$ reaction-rates are measured over the front surface of the fission plate to define a thermal flux profile in X and Y.
- (2) The distribution of the U235 content within the fuel is assessed.
- (3) (1) and (2) are combined to provide a relative fission-rate profile in X and Y;
- (4) The relative fission profile in the Z direction through the fuel is obtained from absolute measurements of fission-rate in the plate as described below.
- (5) The fission-rate profile is normalised to absolute measurements of the fission-rate per NESTOR Watt in the plate which are made in the central strip of the central element at the centre, bottom and halfway between the centre and bottom of the fuel.
- (6) The neutron source distribution is obtained from the absolute fission-rate distribution.

The manganese reaction-rate measurements on the front face of the plate were input to the CRISP code [6] to define the manganese reaction-rate surface covering the plate. From this surface the average manganese reaction-rate within the elements of any source mesh overlaid onto the fission plate can be defined. The fission-rate profile in X and Y is taken as the manganese reaction-rate profile on the front face of the fuel plate. This has been normalised to give a plate power of 1 Watt and the resulting neutron source distribution is shown in Table 4. Constants of $3.121\text{E}10$ fissions per Watt and 2.437 neutrons per fission have been used in this derivation.

The absolute fission-rate in the fuel was found to be between 5% and 16% higher in the strip nearer to NESTOR. This difference is caused by the attenuation of thermal neutrons from NESTOR through the 1mm fuel strips. However, the attenuation of the neutrons produced by fission is small over this distance so an assumption of no Z dependence in the source strength has been made.

The absolute power in the fission plate, expressed as plate Watts per NESTOR watt, has been determined by combining measurements of the absolute fission-rate at spot values, gained by fission product decay line counting, with the fission-rate profile data derived in CRISP. The analysis is rather involved and will not be discussed here : the result was an absolute plate power of $5.68\text{E}-4$ Watts per NESTOR Watt. The uncertainty on the plate power is 8% at the 2 s.d. level.

3. DESCRIPTION OF THE MCBEND CALCULATIONS

MCBEND is a general purpose Monte Carlo radiation shielding code [3]. The code is well suited to the task of benchmarking nuclear data since bias due to geometry and energy modelling is minimised. Version 7B of the code has been used in this work to predict detector count rates along the central axis of the shield array and to predict the sensitivity of detector count rates to the basic nuclear data. The sensitivity results will not be presented in detail here but have been used to evaluate the uncertainties on the calculated results due to uncertainties in the nuclear data.

3.1 Geometry modelling

The geometry of the shield, as shown in Figure 1 and Table 1, was modelled exactly using the Combinatorial Geometry option of MCBEND. The modelling of the fission plate in the axial direction, as shown in Figure 4, was exact ; in the radial direction the fuel, aluminium blanks and clearance gap

thick mild steel plate. The trolley base has a 25 cm high steel chassis in-filled with concrete. The structure of NESTOR surrounding the trolley comprises concrete bulk shielding blocks except on the NESTOR core side of the trolley front face where it is graphite. This graphite extends away from the trolley to the external graphite reflector of the reactor. Table 2 gives the compositions of the materials used in the experiment.

2.3 Activation detector measurements in the iron 88 benchmark

The neutron distribution through the experimental shield has been mapped using activation foils attached to thin aluminium carriers (0.5 mm thick by 9 cm wide) located between the slab components. The detector set comprised activation foils to measure the epi-cadmium $\text{Au}^{197}(\text{n},\gamma)\text{Au}^{198}$ reaction-rate and the $\text{S}^{32}(\text{n},\text{p})\text{P}^{32}$, $\text{In}^{115}(\text{n},\text{n}')\text{In}^{115\text{m}}$, $\text{Rh}^{103}(\text{n},\text{n}')\text{Rh}^{103\text{m}}$ and $\text{Al}^{27}(\text{n},\alpha)\text{Na}^{24}$ threshold reaction-rates. Penetration measurements were made along the nuclear centre line, which is the horizontal axis of the system passing through the centre of the fission plate. Lateral distributions were also measured at various positions in the shields, the foils being located at intervals of 25cm up and down from the nuclear centre line. The labelling convention for the measurement locations is given in Figure 2. Data pertaining to the activation foils (ie size, calibration uncertainty) are given in Table 3.

A fraction of the neutrons present in the experimental array originate from leakage from the NESTOR core. To obtain a true comparison between measurement and a calculation using the fission plate source, the NESTOR core component must be subtracted from the measurement. There are two methods by which the background component can be estimated.

The best method is to repeat the measurement with the fissile content of the fission plate removed, ie an unfuelled measurement. This is a time consuming method as measurements have to be made twice at every point, once with the fuel and once without. The combination of low fluxes and low sensitivities of integral detectors can make foreground fuelled measurements difficult at deep penetration with the result that unfuelled measurements become impossible.

Background corrections of acceptable accuracy can be made for the high energy threshold reactions by a second method using the hydrogen filled proportional counters of the TNS system [5] in integral mode. Here measurements of the neutron count-rates in the shield with the ASPIS shutter open and closed are required together with a measure of the shut-down ratio of the fission plate when the neutron shutter is closed. This technique has been used for determining the background correction for the proportional counters ; the correction was found to be around 2% throughout the shield and a value of 2% is recommended for the four threshold detectors at all positions in the shield.

The unfuelled technique for background correction has been adopted for the gold measurements as there is a significant component of the low energy flux which does not arise from the fission plate particularly near the fission plate itself where the fuelled to unfuelled ratio can be as low as 3.

2.4 Source description

A schematic diagram of the fission plate is shown in Figure 3. It comprises an aluminium frame which fills the height and width of the ASPIS trolley. Located within the frame are 13 separate fuel elements. A schematic view of an individual fuel element is shown in Figure 4. Each element has two 12 mm thick aluminium cover plates which attach on either side of the top and bottom locating end pieces leaving a 5 mm separation in which U/Al alloy fuel strips are located. The fuel strips are 80% by weight aluminium and 20% by weight of uranium enriched to 93% having a density of 3.256 g/cm^3 . Each strip is nominally 30.5 mm wide and 1 mm thick and is fixed to the rear cover plate by M5 screws.

Three columns of fuel strips laid side by side fill the width of the element. There is depth for 4 fuel strips within each element leaving a 1 mm clearance gap next to the front cover plate. In the current configuration only the central two strips in each column contain U/Al alloy, the outer two are both blanks manufactured from aluminium. To approximate to a disc fission neutron source the axial fuel

loading within each element has been arranged to the specification shown in Figure 5 by the substitution of aluminium blanks where necessary.

The approach taken to obtain the absolute power distribution within the fission plate is summarised as follows:

- (1) $\text{Mn55}(n,\gamma)\text{Mn56}$ reaction-rates are measured over the front surface of the fission plate to define a thermal flux profile in X and Y.
- (2) The distribution of the U235 content within the fuel is assessed.
- (3) (1) and (2) are combined to provide a relative fission-rate profile in X and Y;
- (4) The relative fission profile in the Z direction through the fuel is obtained from absolute measurements of fission-rate in the plate as described below.
- (5) The fission-rate profile is normalised to absolute measurements of the fission-rate per NESTOR Watt in the plate which are made in the central strip of the central element at the centre, bottom and halfway between the centre and bottom of the fuel.
- (6) The neutron source distribution is obtained from the absolute fission-rate distribution.

The manganese reaction-rate measurements on the front face of the plate were input to the CRISP code [6] to define the manganese reaction-rate surface covering the plate. From this surface the average manganese reaction-rate within the elements of any source mesh overlaid onto the fission plate can be defined. The fission-rate profile in X and Y is taken as the manganese reaction-rate profile on the front face of the fuel plate. This has been normalised to give a plate power of 1 Watt and the resulting neutron source distribution is shown in Table 4. Constants of $3.121\text{E}10$ fissions per Watt and 2.437 neutrons per fission have been used in this derivation.

The absolute fission-rate in the fuel was found to be between 5% and 16% higher in the strip nearer to NESTOR. This difference is caused by the attenuation of thermal neutrons from NESTOR through the 1mm fuel strips. However, the attenuation of the neutrons produced by fission is small over this distance so an assumption of no Z dependence in the source strength has been made.

The absolute power in the fission plate, expressed as plate Watts per NESTOR watt, has been determined by combining measurements of the absolute fission-rate at spot values, gained by fission product decay line counting, with the fission-rate profile data derived in CRISP. The analysis is rather involved and will not be discussed here : the result was an absolute plate power of $5.68\text{E}-4$ Watts per NESTOR Watt. The uncertainty on the plate power is 8% at the 2 s.d. level.

3. DESCRIPTION OF THE MCBEND CALCULATIONS

MCBEND is a general purpose Monte Carlo radiation shielding code [3]. The code is well suited to the task of benchmarking nuclear data since bias due to geometry and energy modelling is minimised. Version 7B of the code has been used in this work to predict detector count rates along the central axis of the shield array and to predict the sensitivity of detector count rates to the basic nuclear data. The sensitivity results will not be presented in detail here but have been used to evaluate the uncertainties on the calculated results due to uncertainties in the nuclear data.

3.1 Geometry modelling

The geometry of the shield, as shown in Figure 1 and Table 1, was modelled exactly using the Combinatorial Geometry option of MCBEND. The modelling of the fission plate in the axial direction, as shown in Figure 4, was exact ; in the radial direction the fuel, aluminium blanks and clearance gap

were modelled as discs of radius 60 cm. Preliminary runs showed that if the model behind the fission plate (i.e. towards NESTOR from the fission plate) only extends to the end of the trolley then the prediction of the low energy flux in the first five measuring positions is too low, resulting in low C/M values for the gold detector. The model in this region was extended by including a 1m long graphite region to represent the region of NESTOR behind the trolley face. All of the calculations with JEF2.2 data reported here used this extended model but the calculations with UKNDL data (performed previously) used the shorter model and hence results for the gold detector in the first five positions are not quoted for calculations with UKNDL data. Inspection of the particle population shows that the extra graphite region is sufficiently long to model the experiment accurately.

3.2 Source modelling

The source profile in the X-Y mesh as shown in Table 4, was modelled exactly in the calculations with uniform distribution in Z. The source strength from this profile is equivalent to 1 plate Watt : the calculated results have been normalised to 30kW NESTOR power using the experimentally determined factor of 5.68E-4 plate Watts per NESTOR Watt. The spectrum for the calculations was taken as the Watt-Cranberg fission spectrum which is built into MCBEND.

3.3 Material modelling

The composition of the materials in the experiment was modelled exactly, as shown in Table 2. JEF2.2 data does not contain natural elements but only isotopes. Thus for Fe, Cr and Ni the natural element had to be divided into isotopic content. Table 5 shows the weight proportions of each isotope which were used in this work. The lack of data for natural elements is, from the user's viewpoint, a major drawback of the JEF2.2 data and it is to be hoped that future JEF libraries will contain natural elements. Table 6 gives the JEF2.2 material numbers which were used for each isotope.

3.4 Variance reduction

The standard MCBEND technique of splitting and Russian Roulette [7] was used to accelerate the calculations. The wide range of detector energies meant that a number of calculations had to be performed to obtain high precision on all detector count rates within a reasonable cpu time. One run used the sulphur detector as the target response, a second used the rhodium detector (and calculated the indium detector count rate with satisfactory efficiency too), a third aimed at the gold detector and a fourth used the aluminium detector as the target response. The automatic acceleration option of MCBEND (MAGIC [8]) was used to provide the importances for splitting/Russian roulette, with target regions placed along the central axis in the gaps between the plates and in the plates themselves. The adjoint source strength at each target region was simply the inverse of the detector reaction-rate corresponding to that region ; in this way the calculation is optimised for all measurement positions along the axis.

3.5 Nuclear data

The nuclear data for the MCBEND calculation is held in 8220 energy groups. This group scheme is used both for criticality and shielding calculations and is particularly fine below 72 eV in order to represent the resonance structure in heavy elements. In the energy region from 72 eV upwards the groups each have a lethargy width of $1/128$. The JEF2.2 data was processed into the 8220 group scheme using the NJOY89.62W code [9,10]. The following resonance shielding treatments were used:

All nuclides except Fe56, U235 and U238
U235 and U238
Fe56

Infinitely dilute method
Subgroup method
Infinitely dilute, totally shielded or
subgroup method.

The following global flux spectrum was used in processing all cases :

$1/E$ above 1 eV
Constant between 1 eV and 0.0253 eV
 E below 0.0253 eV

The "totally shielded" cross-sections were obtained with a zero background cross-section (i.e. by weighting with the reciprocal of the nuclide total cross-section). In the subgroup method, pairs of groups from the 8220 group scheme were combined and cross-sections for two subgroups were generated and used as the values in the two original groups. Details of the method are given in Reference 11.

For simplicity, the following sections will refer to the different types of data as "dilute", "shielded" or "subgroup". Note, however, that this will apply specifically to the differences in the Fe56 treatment ; the methods used for the other nuclides in this study are fixed as specified above.

The object of producing the three different versions of the Fe56 data was to examine the sensitivity of the results to the resonance shielding treatment. The difference between the results obtained with infinite dilution and totally shielded cross-sections gives an indication of whether, with this group scheme, resonance shielding corrections have a significant effect. Differences between results obtained with infinite dilution and totally shielded cross-sections indicate that the group scheme is not fine enough to be equivalent to point energy. Totally shielded cross-sections using $1/(E\Sigma_T)$ are appropriate to slowing down in a material whereas shield calculations involve penetration through a region. The correct weighting spectrum is thus spatially dependent and neither $1/E$ nor $1/(E\Sigma_T)$ are correct even for materials with single isotopes. However, when the energy group scheme is not equivalent to point energy then the use of the totally shielded cross-section is the best available approximation. The subgroup method should, in principle, be able to produce the appropriate resonance shielding effect in a range of systems in which iron is present in different proportions (e.g. in mild steel, in stainless steel and in multi-material shields). It must therefore be tested for a variety of cases, and it is included in this analysis as one of these tests.

In view of the above considerations, the "shielded" data will be regarded as the first choice or "recommended" set for this benchmark, and the most detailed analysis will be carried out with this set.

3.6 Detector cross-sections

The detector cross-sections, or "response functions" used to evaluate the $S32(n,p)P32$, $In115(n,n')In115m$, $Rh103(n,n')Rh103m$ and $Al27(n,\alpha)Na24$ reaction rates were taken from the MCBEND response function library which contains these responses in 620 groups and is sourced from the IRDF dosimetry file [12]. The response function for the $Au197(n,\gamma)Au198/Cd$ reaction rate was in suppressed form, specific to the thickness of the detector foils which were used and is shown in Table 7. The suppressed resonance integral for the response function given in Table 7 has been calculated and found to be 4.6% higher than the measured suppressed resonance integral [13]. Thus an extra suppression factor of 4.6% has been applied to the $Au197(n,\gamma)Au198/Cd$ detector results.

3.7 Details of the MCBEND runs

The JEF2.2 calculations for the sulphur, rhodium/indium and gold detectors were run with "dilute", "shielded" and "subgroup" data whilst the calculation for the aluminium detector was only run with "dilute" data, making 10 calculations in total. These calculations were all run on SUN workstations, with a total cpu time on a Sparc IPX of 497 hours. Monte Carlo standard deviations on the responses were generally less than 3%. This benchmark has previously been analysed with UKNDL data [14] and the results will be shown here for comparison. Note that for the UKNDL data (also in 8220 groups) all elements except U235 and U238 use the "shielded" method for evaluating group-averaged cross-sections.

4. DISCUSSION OF THE RESULTS

The measured and predicted $S32(n,p)P32$, $In115(n,n')In115m$, $Rh103(n,n')Rh103m$, $Au197(n,\gamma)Au198/Cd$ and $Al27(n,\alpha)Na24$ reaction rates are given in Tables 8-12, respectively. Each table includes the experimental results, the MCBEND predictions using UKNDL data and the MCBEND predictions using JEF2.2 "dilute" data, JEF2.2 "shielded" data and JEF2.2 "subgroup" data. Figures 6-10 show the reaction rate vs. shield thickness profile for the measurements, the UKNDL predictions and the JEF2.2 "shielded" predictions. Tables 13-17 give the C/M values for each detector and Figures 11-15 show these results for UKNDL and JEF2.2 "shielded" data.

The experimental results for the gold detector have been corrected for background radiation leaking from NESTOR. The correction for the threshold detectors is 2% throughout the shield and is small compared with the uncertainty due to the source strength (8% at the 2 s.d. level) and so has not been applied. This correction would not affect the conclusions drawn from the results.

The uncertainties quoted in the reaction rate tables and figures are at the one s.d. level and are due to counting statistics or Monte Carlo stochastic error. The uncertainties quoted in the C/M tables and graphs are at the 2 s.d. level and are due to the same uncertainties. Further experimental uncertainties arising from detector calibration are listed with each table. Further calculational uncertainties are given in Table 18 and discussed in detail in section 4.6.

The results for each detector will be discussed in turn in sections 4.1 to 4.5, followed by a discussion of the uncertainties on the calculation in section 4.6. The results using the different methods of evaluating group-averaged Fe56 data will be discussed in section 4.7 whilst in section 4.8 the results discussed in the previous sections, together with sensitivity results, will be used to draw inferences about the JEF2.2 data.

4.1 $S32(n,p)P32$ detector

Table 13 shows that the UKNDL data severely overpredicts the attenuation of the $S32(n,p)P32$ reaction rate through the shield, with C/M falling from 0.89 at the fission plate to 0.55 after 67 cm of mild steel. The JEF2.2 "dilute" data performs much better, with most C/M values being within 2 s.d. of unity. There is some underprediction near the fission plate which is also observed with the other datasets and has been observed throughout another experimental programme using the same fission plate. This underprediction could partly be due to the 10% uncertainty (at the 2 s.d. level) in the calibration of the sulphur detectors. The JEF2.2 "shielded" and "subgroup" data give similar results, showing the previously mentioned underprediction at the fission plate, good predictions for shield depths between 10 cm and 41 cm and some overpredictions beyond 41 cm. The C/M for the "shielded" set varies from 0.90 at the fission plate to 1.14 after 57 cm. The results using "shielded" and "subgroup" data are higher than those using the JEF2.2 "dilute" data. A discussion of the results obtained using the three different methods of processing Fe56 group-averaged cross-sections is given in section 4.7. The recommended JEF2.2 data is the "shielded" set. Thus the JEF2.2 data slightly underpredicts the attenuation through the shield but performs much better than the UKNDL data, as shown in Figures 6 and 11.

4.2 $In115(n,n')In115m$ detector

Table 14 shows that the UKNDL data severely overpredicts the attenuation of the $In115(n,n')In115m$ reaction rate through the shield, with C/M decreasing from 0.94 at the fission plate to 0.41 after 46 cm of mild steel. The JEF2.2 "dilute" data gives similarly poor results, with the C/M decreasing from 0.92 to 0.40 over the same range. JEF2.2 "shielded" and "subgroup" data give somewhat better results: the attenuation is still overpredicted but not as severely as with UKNDL and JEF2.2 "dilute" data. The C/M for the JEF2.2 "shielded" data decreases from 0.91 at the fission plate to 0.62 after 46 cm of mild steel. Experimental results were not available beyond 46 cm into the shield but the trend up to that point indicates that C/M values would be very low at the back of the shield (for example, one can extrapolate to a C/M value of around 0.5 after 62 cm of mild steel using JEF2.2 "shielded" data). The "shielded" and "subgroup" JEF2.2 data produce much higher results than the "dilute" data: this is discussed further in section 4.6. The recommended JEF2.2 data ("shielded") clearly performs better

than the UKNDL data, as shown in Figures 7 and 12, but the low C/M values indicate a possible problem with the basic JEF2.2 data.

4.3 Rh103(n,n')Rh103m detector

Table 15 shows that the UKNDL data overpredicts the attenuation of the Rh103(n,n')Rh103m reaction rate through the shield, with C/M decreasing from 0.98 at the fission plate to 0.73 after 62 cm of mild steel. The overprediction is not, however, as severe as that observed for the sulphur and indium detectors. The JEF2.2 "dilute" data performs worse, with C/M decreasing from 0.96 to 0.59 over the same range. The JEF2.2 "shielded" and "subgroup" data both give similar results which are a large improvement over the "dilute" results and some improvement over the UKNDL results. For JEF2.2 "shielded" data the attenuation is very slightly overpredicted, with C/M decreasing to 0.90 after 62 cm of mild steel (minimum value 0.88). Again the "shielded" and "subgroup" results are significantly higher than the "dilute" results - see section 4.6 for more discussion. The recommended JEF2.2 data ("shielded") performs well, with a slight overprediction of attenuation, and is better than the UKNDL data, as shown in Figures 8 and 13.

4.4 Au197(n, γ)Au198/Cd detector

Table 16 shows that the UKNDL data underpredicts the Au197(n, γ)Au198/Cd reaction rate by 10-20% in the shield but predicts the attenuation reasonably well, with C/M values fluctuating around a mean of 0.84. The JEF2.2 "dilute" data gives consistent results up to 31 cm into the shield and then underpredicts the reaction rate. The attenuation is fairly well predicted, except at the end of the shield where the C/M drops to 0.80. The JEF2.2 "shielded" data gives C/M results which are within 2 s.d. of unity. The results at positions A11 and A12 are high with high standard deviations. These anomalous results (probably due to a high weight particle) are an indication of the difficulty of variance reduction for this detector. However, on an examination of the calculated fluxes, it is considered that the results at other positions are reliable (i.e. not wildly inaccurate). The JEF2.2 "subgroup" data gives results which lie between the "dilute" and "shielded" data, with C/M values which are within 2 s.d. of unity up to 31 cm into the shield and thereafter vary between 0.88 and 0.92. The recommended JEF2.2 data ("shielded") again performs better than the UKNDL data, as shown in Figures 9 and 14.

4.5 Al27(n, α)Na24 detector

Table 17 shows that the UKNDL data tends to overpredict the Al27(n, α)Na24 reaction rate but the standard deviations are rather high (no separate run was performed for this detector using UKNDL data) so definite conclusions cannot be drawn. The JEF2.2 "dilute" data gives C/M values which are generally within 2 s.d. of unity with a slight underprediction after 26 cm of mild steel. These results seem better than the UKNDL results but the high standard deviations on the UKNDL results together with the low number of experimental points (four) again make definite conclusions difficult.

4.6 Discussion of total calculational uncertainty

There are various sources of calculational uncertainty, including uncertainty in source strength, uncertainties in the nuclear data, uncertainties in the detector cross-sections, uncertainties in the effective mass (density multiplied by thickness) of each slab, approximations in the model, uncertainties in the source spectrum and Monte Carlo statistics. Table 18 gives a summary of the uncertainties on the calculated reaction-rates for each detector at two positions in the shield. (Note that the two positions are not the same for all detectors).

The uncertainty in the source strength has been measured to be 8% at the 2 s.d. level and this uncertainty applies directly to the calculated results.

The uncertainties in the nuclear data are given in the form of variance-covariance matrices. These matrices are not yet available for JEF2 data but are available for JEF1 data [15]. The JEF1 variance-covariance data for iron and carbon have been used in this work, together with sensitivities calculated by MCBEND, to evaluate the uncertainty on the reaction-rates due to uncertainties in the data for these

elements. Table 18 shows that the uncertainties due to uncertainties in the carbon data are negligible. The uncertainties caused by uncertainties in the iron data are small next to the fission plate (position A2), as one would expect, but are larger at medium to deep penetration. They are particularly large for the $S32(n,p)P32$, $In115(n,n')In115m$ and $Al27(n,\alpha)Na24$ detectors with values of around 61%, 27% and 40% for these detectors after 66 cm, 46 cm and 26 cm of penetration, respectively. This reflects a large uncertainty in the iron data coupled with high sensitivities. The values for the $Rh103(n,n')Rh103m$ and $Au197(n,\gamma)Au198/Cd$ detectors are around 11% after 66 cm of penetration.

The uncertainties on the detector cross-sections were based on recommendations by McCracken [16] and are given in Table 19. Values were not available for the indium and aluminium detectors. These uncertainties are combined with sensitivities of the reaction-rates to each flux scoring group to produce uncertainties in the calculated reaction-rates between 5% and 15% throughout the shield. The threshold detectors have broadly similar values which increase through the shield whilst the values for gold are lower and are roughly constant through the shield.

The uncertainty on the effective mass of each slab was estimated from uncertainties on the mass of each slab and on the lateral dimensions of the slab. Note that uncertainty on the thickness of the slab is irrelevant since the product of density and thickness contains no thickness term. The uncertainty on the effective mass of the whole shield was found to be 0.1% which when multiplied by the sensitivity to the iron cross-section gives the uncertainty on the calculated reaction-rates. The values obtained were all small compared with other calculation uncertainties.

There is a small approximation in the modelling of the geometry of the source material, but not the source strength. The fuel, as described in section 3.2, was modelled as a disc of radius 60 cm. Thus over a region (7 cm - 8 cm) outside the boundaries of the real fuel the model contains fuel material instead of aluminium. The uncertainty caused by this approximation has not been quantified but since the fuel is only 2mm thick an assumption of negligible uncertainty has been made.

The uncertainty in the $U235$ fission spectrum is small below 4 MeV but is higher at the high energy tail. An estimate of the uncertainty in the calculated values for each detector due to this uncertainty has been made by estimating the difference in reaction-rate caused by using two spectra with different values of the fitting parameters and taking twice the s.d. of the two results. The difference in the reaction-rate has been estimated by finding the weighted mean of the differences between the spectra where the weighting function is the proportion of the spectrum in the particular energy group multiplied by the importance of that energy group for the reaction-rate in question. The results show that the uncertainties in the calculation decrease with the threshold energy of the detector. This is as one would expect since the higher energy threshold detectors are more sensitive to the high energy tail of the fission spectrum where the uncertainty is greatest. The values vary between around 15% and 0.5%.

The Monte Carlo statistics translate directly into uncertainties on the calculation and are under 10% (at the 2 s.d. level) for all detectors.

The total calculational uncertainty for the $S32(n,p)P32$, $In115(n,n')In115m$ and $Al27(n,\alpha)Na24$ detectors at penetrations of 66 cm, 46 cm and 26 cm, respectively, is 63%, 32% and 47%. These are dominated by the uncertainty due to uncertainty in the iron data. For the $Rh103(n,n')Rh103m$ detector the uncertainty at the back of the shield is 21% and has large contribution from detector cross-section uncertainty and uncertainties in the iron data. For the $Au197(n,\gamma)Au198/Cd$ detector the total uncertainty in this position is 16% and is mainly due to uncertainties in the iron data and uncertainties in the source strength.

4.7 Comparison of the different methods of evaluating the group-averaged Fe56 cross-section

Table 20 shows the ratio of results obtained using JEF2.2 "shielded" data and JEF2.2 "dilute" data and Table 21 shows a similar comparison for the "subgroup" and "dilute" data. The results using "subgroup" data generally follow those using "shielded" data. There is clearly a significant difference between results using "dilute" data and "shielded" data and also between results using "dilute" data and "subgroup" data. These differences indicate that for deep penetration in iron the group structure in

which the data is held ($1/128$ lethargy width) is not fine enough to eliminate dependence on the weighting flux used to collapse the data within the group. The problem occurs in the Fe56 resonance region between 0.01 MeV and 3 MeV. The indium and rhodium detectors, with thresholds at approximately 0.4 MeV and 0.1 MeV, respectively, are particularly sensitive to this region as reflected in the large difference between results using "dilute" data and "shielded" data and between results using "dilute" data and "subgroup" data. The sulphur detector is less affected since its threshold is at approximately 2 MeV. The gold detector is also affected since it is sensitive to epithermal neutrons produced by slowing down from the critical energy range. The aluminium detector, with a threshold of around 6 MeV, should not be affected. Part of the Fe56 resonance region (0.01 - 0.86 MeV) consists of resolved resonances but part (0.86 - 3 MeV) consists of unresolved resonances.

The fact that the "subgroup" data give results similar to those from the "shielded" data for this benchmark is to be expected since the nuclide in question is present in a high concentration (92% by weight). This also means that, as discussed in section 3.5, these data would be expected to be more appropriate than the infinite dilution values in this system, and in fact they did give better overall agreement with the measurements. The performance of the "shielded" data is discussed in more detail in section 4.8.

This analysis has demonstrated, by reference to the extreme case of deep penetration in iron, that one cannot always neglect the effects of resonance shielding on the cross-sections in the upper energy range of the 8220 group scheme. However, the groups in this range are still very fine: $1/128$ lethargy width corresponds to 90 groups between 1 and 2 MeV, for example. Therefore a simple procedure such as the 2-subgroup method described in this report is probably all that is necessary to provide an adequate system-independent cross-section set for a nuclide such as iron. The method has operated adequately for this benchmark but requires further testing on a wider range of systems. These tests would ideally include the generation of data in a finer group scheme; this would provide a reference against which to test the existing scheme and it could form the basis of a new group scheme if improved accuracy is required.

4.8 Assessment of the JEF2.2 data

The foregoing sections have shown that the JEF2.2 data with the "shielded" method of producing group-averaged Fe56 cross-sections performs better than the UKNDL data for all of the detectors considered. The JEF2.2 "shielded" data very slightly underpredict the attenuation of the S32(n,p)P32 reaction rate through the shield, slightly overpredict the attenuation of the Rh103(n,n')Rh103m reaction rate, quite markedly overpredict the attenuation of the In115(n,n')In115m reaction rate and predict the attenuation of the Au197(n, γ)Au198/Cd reaction rate reasonably well. It is worth noting that the C/M results for the S32(n,p)P32, Rh103(n,n')Rh103m and Au197(n, γ)Au198/Cd detectors lie well within the total calculational uncertainties given in Table 18. This may indicate that some of the uncertainties used to calculate total calculational uncertainty may be too large. However, the results for the In115(n,n')In115m detector do not lie within the total calculational uncertainty and this indicates that there may be a deficiency in the basic nuclear data.

Sensitivities of the S32(n,p)P32, In115(n,n')In115m and Rh103(n,n')Rh103m reaction rates to the Fe56 elastic and nonelastic cross-sections are shown in Figures 16-18. The S32(n,p)P32 reaction rate is very sensitive to the nonelastic cross-section between 2.6 MeV and 4.4 MeV and is also fairly sensitive to the elastic cross-section in this energy range and to both nonelastic and elastic cross-sections between 1.35 MeV and 2.6 MeV. One of the conclusions from the original UKNDL work was that the iron nonelastic cross-section between 1.35 MeV and 4.4 MeV was possibly 11-14% too high, resulting in the low C/M values for the sulphur detector [14]. The much improved C/M values for the sulphur detector indicate that this possible deficiency in the basic UKNDL data may have been corrected in the JEF2.2 data.

The In115(n,n')In115m and Rh103(n,n')Rh103m reaction rates are both very sensitive to the elastic cross-section between 0.58 MeV and 0.71 MeV with the indium detector being nearly twice as sensitive as the rhodium. The In115(n,n')In115m reaction rate is also sensitive to both elastic and nonelastic cross-sections between 0.71 MeV and 2.6 MeV whereas the Rh103(n,n')Rh103m reaction rate is not particularly sensitive to the cross-sections in this energy range. The Rh103(n,n')Rh103m

reaction rate, as one would expect, is fairly sensitive to the elastic cross-sections between 0.26 MeV and 0.58 MeV ; in this range the $\text{In115}(n,n')\text{In115m}$ reaction rate is only sensitive to the elastic cross-section between 0.41 MeV and 0.58 MeV. The fact that the attenuation of the $\text{In115}(n,n')\text{In115m}$ reaction rate is markedly overpredicted whilst that of the $\text{Rh103}(n,n')\text{Rh103m}$ reaction rate is only slightly overpredicted, together with the fact that the $\text{In115}(n,n')\text{In115m}$ reaction rate is much more sensitive to cross-sections in the 0.58 MeV to 2.6 MeV energy range indicates that there could be possible deficiencies in the Fe56 data in this range. However, since the $\text{S32}(n,p)\text{P32}$ reaction rate is reasonably well predicted at the back of the shield and is sensitive to the cross-sections in the 1.35 MeV to 2.6 MeV range, the range in which there might be a deficiency in the data should be reduced to 0.58 MeV to 1.35 MeV. However, as the results show that the data used in MCBEND in 8220 groups is sensitive to the weighting spectrum it is not possible to differentiate between deficiencies in the JEF2.2 data and shortcomings in the group processing.

5. CONCLUSIONS

- i) The iron 88 single material benchmark experiment has been analysed using the Monte Carlo code MCBEND with JEF2.2 data as part of a programme of JEF2.2 data benchmarking for shielding calculations.
- ii) Three methods of evaluating the group-averaged Fe56 cross-section were used in this work. Comparison of the results obtained using the three methods indicates that the group scheme used to hold the nuclear data ($1/128$ lethargy width) in the Fe56 resonance region (0.01 MeV to 3 MeV) is not fine enough to remove all dependence on resonance shielding. Two of the methods gave very similar results : total shielding and a simple subgroup method. Both of these gave better overall agreement with the measurements than infinite dilution cross-sections.
- iii) Comparison of results using the JEF2.2 data with totally self-shielded Fe56 and those obtained using UKNDL data show that for all detectors considered ($\text{S32}(n,p)\text{P32}$, $\text{In115}(n,n')\text{In115m}$, $\text{Rh103}(n,n')\text{Rh103m}$, $\text{Au197}(n,\gamma)\text{Au198/Cd}$ and $\text{Al27}(n,\alpha)\text{Na24}$) the JEF2.2 data performs better than the UKNDL data.
- iv) The JEF2.2 results for the sulphur, rhodium and gold detectors are reasonably good (i.e. slight underprediction or overprediction of attenuation). Those for the indium detector, however, show a marked overprediction of the attenuation.
- v) The good results for the sulphur detector indicate that the problem with the UKNDL Fe56 nonelastic cross-section in the 1.35 MeV to 4.4 MeV range possibly being too high may have been corrected in JEF2.2 data.
- vi) The poor results for the indium detector in contrast to good results for the sulphur and rhodium detectors, when considered in conjunction with the sensitivity results, indicate a possible deficiency in the JEF2.2 Fe56 data in the 0.58 MeV to 1.35 MeV energy range.
- vii) The lack of natural element data in JEF2.2 is a major drawback from the user's viewpoint.
- viii) The "subgroup" method and the use of finer group schemes should be tested as possible approaches to use in practical shielding calculations.

14090477

REFERENCES

1. C.Nordborg, H.Gruppelaar and M.Salvatores "Status of the JEF and EFF projects" Proc. Int. Conf. on Nuclear Data for Science and Technology, Fed. Rep. Germany, May 1991
2. C.Nordborg "Distribution of JEF2.2" JEF/DOC-371, 1992
3. MCBEND User Guide to Version 7 ANSWERS/MCBEND(91)7
4. H.F.Locke and G.A.Wright "Benchmark testing of JEF2.2 data for shielding applications : analysis of the Winfrith water benchmark experiment" AEA-RS-1232, 1993
5. M.J.Armishaw, J.Butler, M.D.Carter, I.J.Curl and A.K.McCracken "A transportable neutron spectrometer (TNS) for radiological applications" AEEW-M2365, 1986
6. I.J.Curl "CRISP - A computer code to define fission plate source profiles" RPD/IJC/934
7. E.Shuttleworth "An introduction to the Monte Carlo method as applied in the radiation transport code MCBEND" ANSWERS(MCBEND)14
8. The use of the MAGIC module for accelerating MCBEND ANSWERS/MCBEND(90)1
9. R.E.Macfarlane "Introducing NJOY89" Proc. Seminar on NJOY and THEMIS, Saclay, June 1989
10. C.R.Eaton, R.J.Perry and C.J.Dean "Modifications to NJOY89.62 made at Winfrith" LWPC/P(91)38
11. C.J.Dean and C.R.Eaton "Cross-section libraries for ECCO and MONK" Proc. Seminar on NJOY and THEMIS, Saclay, June 1989
12. D.E.Cullen and P.K.McLaughlin "The International Reactor Dosimetry File (IRDF 85)" IAEA-ND5-41
13. A.Packwood "Notes on epi-cadmium foil measurements and calculations" RP&SG/AP/P(87)60
14. S.Bell, I.J.Curl and G.A.Wright "Analysis of the iron 88 benchmark" PTHD 071, 1990
15. I.Kodeli and E.Sartori "ZZ-VITAMIN-J/COVA NEA1264 Covariance Data Library" OECD/NEADB January 1990
16. A.K.McCracken Private communication

Table 1

Shield dimensions of the iron 88 single material benchmark experiment

Component	Material thickness (cm)	Coordinate at end of region (cm)	Material reference number
Trolley Face	3.18	-16.62	1&2
Void	0.52	-16.10	-
Graphite	15.00	-1.10	3
Void	1.10	0.00	-
Fission Plate	2.90	2.90	4 & 5
Void	0.74	3.64	-
Mild Steel	5.10	8.74	6
Void	0.74	9.48	-
Mild Steel	5.12	14.60	6
Void	0.74	15.34	-
Mild Steel	5.12	20.46	6
Void	0.74	21.20	-
Mild Steel	5.10	26.30	6
Void	0.74	27.04	-
Mild Steel	5.20	32.24	6
Void	0.74	32.98	-
Mild Steel	5.15	38.13	6
Void	0.74	38.87	-
Mild Steel	5.20	44.07	6
Void	0.74	44.81	-
Mild Steel	5.20	50.01	6
Void	0.74	50.75	-
Mild Steel	5.25	56.00	6
Void	0.74	56.74	-
Mild Steel	5.18	61.92	6
Void	0.74	62.66	-
Mild Steel	5.07	67.73	6
Void	0.74	68.47	-
Mild Steel	5.12	73.59	6
Void	0.74	74.33	-
Mild Steel	5.18	79.51	6
Void	0.74	80.25	-
Mild Steel	5.10	85.35	6
Mild Steel	5.25	90.60	6
Mild Steel	5.00	95.60	6
Mild Steel	4.97	100.27	6
Stainless Steel	22.41	122.68	7
Concrete	100.00	222.68	8

Notes :

1. For material compositions see Table 2
2. The trolley face is manufactured from mild steel with a central aluminium 'window' of radius 56.1cm.
3. The construction of the fission plate is shown in Figure 6.
4. All slab components are 182.9 cm wide by 191.0 cm high and fill the full width and height of the ASPIS trolley.

Table 2

Material compositions in the iron 88 single material benchmark experiment

Material	Material Reference no.	Density (g.cm-3)	Element	Weight Fraction
Mild Steel	1	7.835	Fe	0.9865
			Mn	0.0109
			C	0.0022
			Si	0.0004
Aluminium	2	2.700	Al	1.0000
Graphite	3	1.650	C	1.0000
Fuel	4	3.256	Al	0.7998
			U235	0.1864
			U238	0.0138
Aluminium	5	2.666	Fe	0.0056
			Si	0.0015
			Al	0.9929
Mild Steel	6	7.850	Fe	0.9903
			Mn	0.0074
			C	0.0023
Stainless Steel	7	7.917	Fe	0.6695
			Mn	0.0157
			Cr	0.1677
			Ni	0.1166
			C	0.0006
			Si	0.0050
			P	0.0003
			S	0.0002
Concrete	8	2.242	Mo	0.0244
			Fe	0.0141
			Si	0.3369
			Al	0.0340
			H	0.0100
			O	0.5290
			Ca	0.0379
			K	0.0200
			Na	0.0161

Table 3

Activation foil data

Detector	Detector Diameter	Thickness	Typical Mass	Cadmium Cover (inches)	Counting System	Systematic Absolute Calibration (uncertainty)
Au	12.7 mm	0.05 mm	0.12-0.13g	50/1000	NaI	0.9%
Rh	12.7 mm	0.015 mm	0.20g	-	NaI	3.0%
In	38mm	1.63mm	12.79g	-	GeLi detector	1.9%
S Pressed Pellet	38.1 mm	2.41 mm	5g	-	Plastic Scintillator	5.0%
S Cast Pellet	51 mm	5.6 mm	22g	-	Plastic Scintillator	5.0%
Al	50mm	3.1mm	16.72g	-	Ge detector	2.2%

Table 4

Source distribution on fission plate

0	0	0	0	0	0	2.973	2.994	2.865	0	0	0	0	0	0
0	0	0	0	0	3.173	3.496	3.537	3.404	2.975	0	0	0	0	0
0	0	0	0	3.176	3.711	4.088	4.149	4.015	3.529	2.890	0	0	0	0
0	0	0	3.186	3.500	4.092	4.514	4.587	4.446	3.925	3.240	2.886	0	0	0
0	0	3.249	3.635	3.999	4.696	5.197	5.286	5.130	4.555	3.807	3.422	3.009	0	0
0	3.150	3.575	4.003	4.412	5.202	5.770	5.870	5.699	5.080	4.282	3.873	3.431	2.970	0
3.040	3.322	3.769	4.223	4.660	5.505	6.110	6.215	6.034	5.387	4.559	4.133	3.673	3.188	2.850
3.132	3.427	3.893	4.364	4.815	5.684	6.304	6.412	6.227	5.563	4.710	4.270	3.792	3.287	2.932
3.026	3.325	3.784	4.239	4.669	5.491	6.079	6.183	6.009	5.364	4.523	4.084	3.607	3.103	2.751
0	3.136	3.574	4.001	4.400	5.157	5.701	5.802	5.643	5.031	4.221	3.795	3.331	2.843	0
0	0	3.182	3.562	3.912	4.572	5.053	5.149	5.013	4.461	3.713	3.317	2.887	0	0
0	0	0	3.004	3.299	3.855	4.267	4.357	4.247	3.766	3.101	2.748	0	0	0
0	0	0	0	2.896	3.396	3.770	3.855	3.758	3.320	2.712	0	0	0	0
0	0	0	0	0	2.745	3.072	3.150	3.067	2.685	0	0	0	0	0
0	0	0	0	0	0	2.458	2.525	2.448	0	0	0	0	0	0

Units are neutrons/cm³/second x 1E7. The plate power for this distribution is 1 Watt.

Coordinate boundaries for source distribution

X	-52.25	-49.08	-45.92	-39.58	-36.42	-30.08	-14.25	-4.75
	4.75	14.25	30.08	36.42	39.58	45.92	49.08	52.25
Y	-51.44	-47.63	-40.64	-35.56	-31.75	-19.69	-15.88	-5.29
	5.29	15.88	19.69	31.75	35.56	40.64	47.63	51.44

Units are cm

Table 5

Division of natural elements into nuclides

Iron		Chromium		Nickel	
Isotope	Weight fraction	Isotope	Weight fraction	Isotope	Weight fraction
Fe54	0.0570	Cr50	0.0417	Ni58	0.6720
Fe56	0.9172	Cr52	0.8370	Ni60	0.2678
Fe57	0.0214	Cr53	0.0967	Ni61	0.0118
Fe58	0.0029	Cr54	0.0245	Ni62	0.0383
-	-	-	-	Ni64	0.0101

Table 6

JEF2.2 material numbers used in the calculations

Nuclide	JEF2.2 material no
Al27	1325
C	600
Ca	2000
Cr50	2425
Cr52	2431
Cr53	2434
Cr54	2437
Fe54	2625
Fe56	2631
Fe57	2634
Fe58	2637
H	10293
Mn55	2525
Mo	4200
Ni58	2825
Ni60	2831
Ni61	2834
Ni62	2837
Ni64	2843
O16	825
Si	1400
U235	9228
U238	9237

Table 7

Suppressed cross-section for 2 thou Au¹⁹⁷(n,γ)Au¹⁹⁸/Cd foils

Lower energy (MeV)	Cross-section (barns)	Lower energy (MeV)	Cross-section (barns)
1.00E1			
8.50E0	1.17E-2	1.50E-3	3.67E0
7.50E0	1.60E-2	1.00E-3	4.48E0
6.50E0	1.50E-2	7.00E-4	5.00E0
5.50E0	1.80E-2	5.00E-4	4.10E0
4.50E0	2.29E-2	3.80E-4	6.89E0
3.50E0	2.98E-2	2.25E-4	1.58E1
2.50E0	4.01E-2	1.50E-4	1.53E1
1.50E0	5.89E-2	1.00E-4	5.16E1
8.50E-1	9.00E-2	7.00E-5	1.22E0
5.00E-1	1.33E-1	5.00E-5	4.41E0
3.50E-1	1.80E-1	3.50E-5	1.31E0
2.25E-1	2.35E-1	2.25E-5	1.45E0
1.50E-1	3.13E-1	1.50E-5	2.53E0
1.00E-1	4.07E-1	1.00E-5	3.90E0
7.00E-2	5.18E-1	7.00E-6	1.30E1
5.00E-2	6.33E-1	5.15E-6	2.37E2
3.50E-2	7.80E-1	4.65E-6	1.514E3
2.25E-2	9.67E-1	3.50E-6	3.09E-2
1.50E-2	1.19E0	2.25E-6	4.98E1
1.00E-2	1.25E0	1.60E-6	2.73E1
7.00E-3	1.49E0	1.30E-6	2.35E1
5.00E-3	1.83E0	1.00E-6	2.29E1
3.50E-3	2.23E0	7.00E-7	2.33E1
2.00E-3	2.89E0	5.50E-7	2.43E1

Table 8

Iron 88 single material benchmark

Measured and predicted S32(n,p)P32 reaction rates

Position	Shield thickness (cm)	Experiment	sd	UKNDL	sd	JEF2 (dilute Fe56)	sd	JEF2 (shielded Fe56)	sd	JEF2 (subgroup Fe56)	sd
A2	0.00	2.02E-17	1.0%	1.79E-17	2.2%	1.84E-17	1.3%	1.81E-17	1.3%	1.79E-17	1.3%
A3	5.10	4.29E-18	1.0%	3.97E-18	2.6%	4.00E-18	1.3%	4.00E-18	1.5%	3.99E-18	1.5%
A4	10.22	1.40E-18	1.0%	1.28E-18	2.7%	1.35E-18	1.3%	1.35E-18	1.6%	1.37E-18	1.6%
A5	15.34	5.12E-19	1.0%	4.33E-19	2.7%	4.96E-19	1.4%	5.03E-19	1.6%	5.13E-19	1.6%
A6	20.44	1.91E-19	1.0%	1.62E-19	2.8%	1.91E-19	1.6%	1.91E-19	1.6%	1.96E-19	1.7%
A7	25.64	7.13E-20	1.0%	5.83E-20	3.0%	7.08E-20	1.6%	7.28E-20	1.8%	7.43E-20	1.7%
A8	30.79	2.70E-20	1.5%	2.15E-20	3.2%	2.68E-20	1.7%	2.80E-20	1.8%	2.86E-20	1.8%
A9	35.99	1.03E-20	1.0%	7.55E-21	3.4%	1.00E-20	1.8%	1.05E-20	1.8%	1.08E-20	1.9%
A10	41.19	3.93E-21	1.0%	3.03E-21	4.3%	3.83E-21	1.8%	4.11E-21	2.0%	4.12E-21	2.1%
A11	46.44	1.49E-21	1.0%	1.05E-21	4.6%	1.45E-21	1.8%	1.61E-21	2.4%	1.63E-21	2.2%
A12	51.62	5.73E-22	1.0%	4.17E-22	4.7%	5.54E-22	2.1%	6.31E-22	2.3%	6.39E-22	2.1%
A13	56.69	2.27E-22	2.5%	1.46E-22	4.5%	2.16E-22	2.3%	2.58E-22	2.6%	2.60E-22	2.6%
A14	61.81	8.53E-23	5.7%	5.37E-22	5.1%	8.21E-23	2.7%	9.28E-23	2.5%	1.02E-22	2.6%
A15	66.99	3.50E-23	20.0%	1.91E-23	5.7%	3.37E-23	3.5%	3.63E-23	3.3%	4.43E-23	5.4%

The quoted standard deviations are due to counting statistics (experiment) or Monte Carlo stochastic error (calculations)

The reaction rates are given in units of reactions per second per atom at 30kW NESTOR power

The three JEF2 results used Fe56 data with different methods of specifying the cross-sections within groups : dilute, shielded or subgroup. These methods are explained in the text.

Table 9

Iron 88 single material benchmark

Measured and predicted In115(n,n')In115m reaction rates

Position	Shield thickness (cm)	Experiment	sd	UKNDL	sd	JEF2 (dilute Fe56)	sd	JEF2 (shielded Fe56)	sd	JEF2 (subgroup Fe56)	sd
A2	0.00	7.02E-17	1.0%	6.63E-17	4.9%	6.44E-17	1.2%	6.37E-17	1.4%	6.37E-17	1.5%
A3	5.10	2.40E-17	1.0%	1.98E-17	6.5%	2.06E-17	1.3%	2.07E-17	1.5%	2.00E-17	1.6%
A4	10.22	1.06E-17	1.0%	7.59E-18	6.6%	8.71E-18	1.4%	8.89E-18	1.5%	8.91E-18	1.7%
A5	15.34	5.14E-18	1.0%	3.35E-18	7.1%	3.92E-18	1.4%	4.14E-18	1.6%	4.12E-18	1.9%
A6	20.44	2.53E-18	1.0%	1.52E-18	8.0%	1.85E-18	1.7%	2.03E-18	1.8%	2.03E-18	2.2%
A7	25.64	1.32E-18	1.0%	8.25E-19	7.1%	8.47E-19	1.8%	9.81E-19	1.9%	9.77E-19	2.0%
A8	30.79	7.21E-19	1.0%	3.82E-19	8.1%	4.09E-19	2.3%	4.99E-19	2.0%	4.96E-19	2.1%
A9	35.99	3.93E-19	1.2%	2.42E-19	13.7%	2.01E-19	2.7%	2.77E-19	6.4%	2.45E-19	2.2%
A10	41.19	2.21E-19	1.4%	9.75E-20	5.9%	1.02E-19	2.6%	1.45E-19	3.5%	1.37E-19	2.7%
A11	46.44	1.28E-19	1.7%	5.27E-20	5.7%	5.14E-20	2.8%	7.93E-20	2.3%	7.69E-20	2.6%
A12	51.62	-	-	2.74E-20	4.9%	2.54E-20	2.9%	4.32E-20	3.3%	4.33E-20	2.9%
A13	56.69	-	-	1.61E-20	5.1%	1.35E-20	2.8%	2.39E-20	2.4%	2.45E-20	2.7%
A14	61.81	-	-	8.38E-21	3.8%	7.79E-21	4.0%	1.45E-20	3.1%	1.48E-20	3.0%
A15	66.99	-	-	5.00E-21	4.5%	4.17E-21	5.3%	8.99E-21	4.1%	9.30E-21	4.2%

The quoted standard deviations are due to counting statistics (experiment) or Monte Carlo stochastic error (calculations)

The reaction rates are given in units of reactions per second per atom at 30kW NESTOR power

The three JEF2 results used Fe56 data with different methods of specifying the cross-sections within groups : dilute, shielded or subgroup. These methods are explained in the text.

Table 10

Iron 88 single material benchmark

Measured and predicted Rh103(n,n')Rh103m reaction rates

Position	Shield thickness (cm)	Experiment	sd	UKNDL	sd	JEF2 (dilute Fe56)	sd	JEF2 (shielded Fe56)	sd	JEF2 (subgroup Fe56)	sd
A2	0.00	3.35E-16	1.0%	3.29E-16	3.8%	3.23E-16	1.0%	3.20E-16	1.1%	3.21E-16	1.2%
A3	5.10	1.42E-16	1.5%	1.39E-16	4.7%	1.36E-16	0.9%	1.41E-16	1.8%	1.34E-16	1.1%
A4	10.22	7.78E-17	1.0%	6.72E-17	4.0%	7.40E-17	0.9%	7.66E-17	1.0%	7.49E-17	1.2%
A5	15.34	4.70E-17	1.0%	3.96E-17	3.8%	4.18E-17	0.9%	4.53E-17	1.0%	4.30E-17	1.1%
A6	20.44	2.86E-17	1.5%	2.46E-17	3.7%	2.49E-17	0.9%	2.81E-17	1.0%	2.68E-17	1.1%
A7	25.64	1.82E-17	1.0%	1.60E-17	3.2%	1.51E-17	1.2%	1.74E-17	1.0%	1.67E-17	1.1%
A8	30.79	1.20E-17	1.0%	1.01E-17	3.0%	9.12E-18	1.0%	1.14E-17	0.9%	1.10E-17	1.2%
A9	35.99	7.97E-18	1.5%	7.93E-18	12.0%	5.84E-18	1.0%	7.62E-18	1.4%	7.19E-18	1.1%
A10	41.19	5.48E-18	1.5%	4.36E-18	2.8%	3.88E-18	1.1%	5.08E-18	1.1%	4.86E-18	1.2%
A11	46.44	3.84E-18	1.5%	3.12E-18	2.6%	2.48E-18	1.3%	3.51E-18	1.1%	3.40E-18	1.3%
A12	51.62	2.68E-18	1.0%	2.01E-18	2.3%	1.70E-18	3.0%	2.38E-18	1.2%	2.36E-18	1.3%
A13	56.69	1.89E-18	1.5%	1.44E-18	2.5%	1.10E-18	1.3%	1.66E-18	1.2%	1.72E-18	1.5%
A14	61.81	1.34E-18	1.0%	9.77E-19	2.1%	7.95E-19	2.2%	1.21E-18	1.4%	1.22E-18	1.7%
A15	66.99	-	-	6.81E-19	2.1%	5.32E-19	2.1%	8.77E-19	1.9%	8.64E-19	2.0%

The quoted standard deviations are due to counting statistics (experiment) or Monte Carlo stochastic error (calculations)

The reaction rates are given in units of reactions per second per atom at 30kW NESTOR power

The three JEF2 results used Fe56 data with different methods of specifying the cross-sections within groups : dilute, shielded or subgroup. These methods are explained in the text.

Table 11

Iron 88 single material benchmark

Measured and predicted Au197(n,γ)Au198/Cd reaction rates

Position	Shield thickness (cm)	Experiment	sd	UKNDL	sd	JEF2 (dilute Fe56)	sd	JEF2 (shielded Fe56)	sd	JEF2 (subgroup Fe56)	sd
A2	0.00	1.05E-14	1.0%	-	-	9.75E-15	3.2%	9.73E-15	4.0%	9.80E-15	3.6%
A3	5.10	6.24E-15	1.0%	-	-	6.06E-15	2.4%	5.87E-15	2.3%	5.88E-15	2.2%
A4	10.22	4.19E-15	1.0%	-	-	4.10E-15	2.2%	4.18E-15	3.3%	4.14E-15	2.0%
A5	15.34	2.97E-15	1.0%	-	-	2.95E-15	2.3%	3.10E-15	2.4%	3.05E-15	2.5%
A6	20.44	2.19E-15	1.0%	-	-	2.17E-15	2.1%	2.31E-15	3.3%	2.22E-15	2.8%
A7	25.64	1.70E-15	1.0%	1.34E-15	2.3%	1.64E-15	2.8%	1.75E-15	1.9%	1.63E-15	2.7%
A8	30.79	1.35E-15	1.0%	1.14E-15	3.1%	1.28E-15	2.4%	1.38E-15	1.7%	1.34E-15	3.8%
A9	35.99	1.11E-15	1.0%	9.68E-16	4.4%	1.03E-15	2.1%	1.11E-15	1.8%	1.02E-15	2.7%
A10	41.19	9.10E-16	1.0%	7.46E-16	2.5%	8.22E-16	2.4%	8.80E-16	1.6%	8.21E-16	2.0%
A11	46.44	7.67E-16	1.0%	6.20E-16	2.4%	7.00E-16	2.2%	8.39E-16	10.5%	6.84E-16	2.2%
A12	51.62	6.55E-16	1.0%	5.18E-16	2.4%	5.72E-16	2.6%	8.04E-16	15.8%	5.72E-16	2.0%
A13	56.69	5.44E-16	1.0%	4.77E-16	2.8%	4.65E-16	2.3%	5.28E-16	2.2%	4.79E-16	1.9%
A14	61.81	4.62E-16	1.0%	3.95E-16	2.0%	3.70E-16	2.0%	4.52E-16	2.8%	4.18E-16	2.2%
A15	66.99	3.99E-16	1.0%	3.66E-16	5.0%	3.18E-16	3.2%	3.72E-16	3.2%	3.68E-16	4.0%

The quoted standard deviations are due to counting statistics (experiment) or Monte Carlo stochastic error (calculations)

The reaction rates are given in units of reactions per second per atom at 30kW NESTOR power

The three JEF2 results used Fe56 data with different methods of specifying the cross-sections within groups : dilute, shielded or subgroup. These methods are explained in the text.

Table 12

Iron 88 single material benchmark

Measured and predicted Al27(n, α)Na24 reaction rates

Position	Shield thickness (cm)	Experiment	sd	UKNDL	sd	JEF2 (dilute Fe56)	sd	JEF2 (shielded Fe56)	sd	JEF2 (subgroup Fe56)	sd
A2	0.00	-	-	1.319E-19	10.8%	1.39E-19	3.2%	-	-	-	-
A3	5.10	2.23E-20	1.0%	2.713E-20	12.2%	2.43E-20	3.5%	-	-	-	-
A4	10.22	-	-	9.069E-21	17.2%	7.25E-21	3.9%	-	-	-	-
A5	15.34	2.55E-21	1.0%	2.769E-21	14.3%	2.50E-21	4.3%	-	-	-	-
A6	20.44	9.56E-22	1.1%	1.112E-21	13.8%	8.96E-22	5.2%	-	-	-	-
A7	25.64	3.56E-22	1.3%	5.615E-22	15.7%	3.16E-22	4.6%	-	-	-	-
A8	30.79	-	-	1.810E-22	17.7%	1.27E-22	9.0%	-	-	-	-
A9	35.99	-	-	6.007E-23	17.6%	-	-	-	-	-	-
A10	41.19	-	-	-	-	-	-	-	-	-	-
A11	46.44	-	-	-	-	-	-	-	-	-	-
A12	51.62	--	-	-	-	-	-	-	-	-	-
A13	56.69	-	-	-	-	-	-	-	-	-	-
A14	61.81	-	-	-	-	-	-	-	-	-	-
A15	66.99	-	-	-	-	-	-	-	-	-	-

The quoted standard deviations are due to counting statistics (experiment) or Monte Carlo stochastic error (calculations)

The reaction rates are given in units of reactions per second per atom at 30kW NESTOR power

The three JEF2 results used Fe56 data with different methods of specifying the cross-sections within groups : dilute, shielded or subgroup. These methods are explained in the text.

14090489

Table 13

Iron 88 single material benchmark

Comparison of measured and predicted S32(n,p)P32 reaction rates

Position	Shield thickness (cm)	UKNDL C/M	Uncertainty (2 sd)	JEF2 (dilute Fe56) C/M	Uncertainty (2 sd)	JEF2 (shielded Fe56) C/M	Uncertainty (2 sd)	JEF2 (subgroup Fe56) C/M	Uncertainty (2 sd)
A2	0.00	0.89	0.04	0.91	0.03	0.90	0.03	0.89	0.03
A3	5.10	0.93	0.05	0.93	0.03	0.93	0.03	0.93	0.03
A4	10.22	0.91	0.05	0.96	0.03	0.96	0.04	0.98	0.04
A5	15.34	0.85	0.05	0.97	0.03	0.98	0.04	1.00	0.04
A6	20.44	0.85	0.05	1.00	0.04	1.00	0.04	1.03	0.04
A7	25.64	0.82	0.05	0.99	0.04	1.02	0.04	1.04	0.04
A8	30.79	0.80	0.06	0.99	0.05	1.04	0.05	1.06	0.05
A9	35.99	0.73	0.05	0.97	0.04	1.02	0.04	1.05	0.05
A10	41.19	0.77	0.07	0.97	0.04	1.05	0.05	1.05	0.05
A11	46.44	0.70	0.07	0.97	0.04	1.08	0.06	1.09	0.05
A12	51.62	0.73	0.07	0.97	0.04	1.10	0.06	1.12	0.05
A13	56.69	0.64	0.07	0.95	0.06	1.14	0.08	1.15	0.08
A14	61.81	0.63	0.10	0.96	0.12	1.09	0.14	1.20	0.15
A15	66.99	0.55	0.23	0.96	0.39	1.04	0.42	1.27	0.52

The quoted uncertainties (2 s.d.) are due to counting statistics (experiment) and Monte Carlo stochastic error (calculations). There are additional systematic experimental uncertainties of 10% on detector calibration at the 2 s.d. level. Calculational uncertainties at selected positions (A2 and A15) are given in Table 18.

The three JEF2 results used Fe56 data with different methods of specifying the cross-sections within groups : dilute, shielded or subgroup. These methods are explained in the text.

Table 14

Iron 88 single material benchmark

Comparison of measured and predicted In115(n,n')In115m reaction rates

Position	Shield thickness (cm)	UKNDL C/M	Uncertainty (2 sd)	JEF2 (dilute Fe56) C/M	Uncertainty (2 sd)	JEF2 (shielded Fe56) C/M	Uncertainty (2 sd)	JEF2 (subgroup Fe56) C/M	Uncertainty (2 sd)
A2	0.00	0.94	0.09	0.92	0.03	0.91	0.03	0.91	0.03
A3	5.10	0.83	0.11	0.86	0.03	0.86	0.03	0.83	0.03
A4	10.22	0.72	0.10	0.82	0.03	0.84	0.03	0.84	0.03
A5	15.34	0.65	0.09	0.76	0.03	0.81	0.03	0.80	0.03
A6	20.44	0.60	0.10	0.73	0.03	0.80	0.03	0.80	0.04
A7	25.64	0.63	0.09	0.64	0.03	0.74	0.03	0.74	0.03
A8	30.79	0.53	0.09	0.57	0.03	0.69	0.03	0.69	0.03
A9	35.99	0.62	0.17	0.51	0.03	0.70	0.09	0.62	0.03
A10	41.19	0.44	0.05	0.46	0.03	0.66	0.05	0.62	0.04
A11	46.44	0.41	0.05	0.40	0.03	0.62	0.04	0.60	0.04
A12	51.62	-	-	-	-	-	-	-	-
A13	56.69	-	-	-	-	-	-	-	-
A14	61.81	-	-	-	-	-	-	-	-
A15	66.99	-	-	-	-	-	-	-	-

The quoted uncertainties (2 s.d.) are due to counting statistics (experiment) and Monte Carlo stochastic error (calculations). There are additional systematic experimental uncertainties of 3.8% on detector calibration at the 2 s.d. level. Calculation uncertainties at selected positions (A2 and A11) are given in Table 18.

The three JEF2 results used Fe56 data with different methods of specifying the cross-sections within groups : dilute, shielded or subgroup. These methods are explained in the text.

Table 15

Iron 88 single material benchmarkComparison of measured and predicted Rh103(n,n')Rh103m reaction rates

Position	Shield thickness (cm)	UKNDL C/M	Uncertainty (2 sd)	JEF2 (dilute Fe56) C/M	Uncertainty (2 sd)	JEF2 (shielded Fe56) C/M	Uncertainty (2 sd)	JEF2 (subgroup Fe56) C/M	Uncertainty (2 sd)
A2	0.00	0.98	0.08	0.96	0.03	0.96	0.03	0.96	0.03
A3	5.10	0.98	0.10	0.96	0.03	0.99	0.05	0.94	0.04
A4	10.22	0.86	0.07	0.95	0.03	0.98	0.03	0.96	0.03
A5	15.34	0.84	0.07	0.89	0.02	0.96	0.03	0.91	0.03
A6	20.44	0.86	0.07	0.87	0.03	0.98	0.04	0.94	0.03
A7	25.64	0.88	0.06	0.83	0.03	0.96	0.03	0.92	0.03
A8	30.79	0.84	0.05	0.76	0.02	0.95	0.03	0.92	0.03
A9	35.99	0.99	0.24	0.73	0.03	0.96	0.04	0.90	0.03
A10	41.19	0.80	0.05	0.71	0.03	0.93	0.03	0.89	0.03
A11	46.44	0.81	0.05	0.65	0.03	0.91	0.03	0.89	0.04
A12	51.62	0.75	0.04	0.63	0.04	0.89	0.03	0.88	0.03
A13	56.69	0.76	0.04	0.58	0.02	0.88	0.03	0.91	0.04
A14	61.81	0.73	0.03	0.59	0.03	0.90	0.03	0.91	0.04
A15	66.99	-	-	-	-	-	-	-	-

The quoted uncertainties (2 s.d.) are due to counting statistics (experiment) and Monte Carlo stochastic error (calculations). There are additional systematic experimental uncertainties of 6% on detector calibration at the 2 s.d. level. Calculation uncertainties at selected positions (A2 and A15) are given in Table 18.

The three JEF2 results used Fe56 data with different methods of specifying the cross-sections within groups : dilute, shielded or subgroup. These methods are explained in the text.

Table 16

Iron 88 single material benchmark

Comparison of measured and predicted Au197(n, γ)Au198/Cd reaction rates

Position	Shield thickness (cm)	UKNDL C/M	Uncertainty (2 sd)	JEF2 (dilute Fe56) C/M	Uncertainty (2 sd)	JEF2 (shielded Fe56) C/M	Uncertainty (2 sd)	JEF2 (subgroup Fe56) C/M	Uncertainty (2 sd)
A2	0.00	-	-	0.93	0.06	0.93	0.08	0.93	0.07
A3	5.10	-	-	0.97	0.05	0.94	0.05	0.94	0.05
A4	10.22	-	-	0.98	0.05	1.00	0.07	0.99	0.04
A5	15.34	-	-	0.99	0.05	1.04	0.05	1.03	0.06
A6	20.44	-	-	0.99	0.05	1.05	0.07	1.01	0.06
A7	25.64	0.79	0.04	0.96	0.06	1.03	0.04	0.96	0.06
A8	30.79	0.84	0.06	0.95	0.05	1.02	0.04	0.99	0.08
A9	35.99	0.87	0.08	0.93	0.04	1.00	0.04	0.92	0.05
A10	41.19	0.82	0.04	0.90	0.05	0.97	0.04	0.90	0.04
A11	46.44	0.81	0.04	0.91	0.04	1.09	0.23	0.89	0.04
A12	51.62	0.79	0.04	0.87	0.05	1.23	0.39	0.87	0.04
A13	56.69	0.88	0.05	0.85	0.04	0.97	0.05	0.88	0.04
A14	61.81	0.85	0.04	0.80	0.04	0.98	0.06	0.90	0.04
A15	66.99	0.92	0.09	0.80	0.05	0.93	0.06	0.92	0.08

The quoted uncertainties (2 s.d.) are due to counting statistics (experiment) and Monte Carlo stochastic error (calculations).

There are additional systematic experimental uncertainties of 1.8% on detector calibration at the 2 s.d. level.

Calculation uncertainties at selected positions (A2 and A15) are given in Table 18.

The three JEF2 results used Fe56 data with different methods of specifying the cross-sections within groups : dilute, shielded or subgroup.

These methods are explained in the text.

Table 17

Iron 88 single material benchmark

Comparison of measured and predicted Al27(n, α)Na24 reaction rates

Position	Shield thickness (cm)	UKNDL C/M	Uncertainty (2 sd)	JEF2 (dilute Fe56) C/M	Uncertainty (2 sd)	JEF2 (shielded Fe56) C/M	Uncertainty (2 sd)	JEF2 (subgroup Fe56) C/M	Uncertainty (2 sd)
A2	0.00	-	-	-	-	-	-	-	-
A3	5.10	1.22	0.30	1.09	0.08	-	-	-	-
A4	10.22	-	-	-	-	-	-	-	-
A5	15.34	1.09	0.31	0.98	0.09	-	-	-	-
A6	20.44	1.16	0.32	0.94	0.10	-	-	-	-
A7	25.64	1.58	0.50	0.89	0.08	-	-	-	-
A8	30.79	-	-	-	-	-	-	-	-
A9	35.99	-	-	-	-	-	-	-	-
A10	41.19	-	-	-	-	-	-	-	-
A11	46.44	-	-	-	-	-	-	-	-
A12	51.62	-	-	-	-	-	-	-	-
A13	56.69	-	-	-	-	-	-	-	-
A14	61.81	-	-	-	-	-	-	-	-
A15	66.99	-	-	-	-	-	-	-	-

The quoted uncertainties (2 s.d.) are due to counting statistics (experiment) and Monte Carlo stochastic error (calculations). There are additional systematic experimental uncertainties of 4.4% on detector calibration at the 2 s.d. level. Calculational uncertainties at selected positions (A2 and A7) are given in Table 18.

The three JEF2 results used Fe56 data with different methods of specifying the cross-sections within groups : dilute, shielded or subgroup. These methods are explained in the text.

Table 18

Total uncertainties on calculated results

Source of uncertainty	Sulphur		Indium		Rhodium		Gold		Aluminium	
	A2	A15	A2	A11	A2	A15	A2	A15	A2	A7
Source strength	8.0%	8.0%	8.0%	8.0%	8.0%	8.0%	8.0%	8.0%	8.0%	8.0%
Iron nuclear data	1.3%	60.6%	1.9%	26.6%	1.6%	10.6%	2.4%	10.6%	1.0%	39.8%
Carbon nuclear data	0.2%	0.4%	0.1%	0.2%	0.1%	0.2%	0.6%	0.2%	0.4%	0.8%
Detector cross-sections	10.2%	14.8%	8.0%*	15.0%*	6.0%	15.2%	5.2%	5.0%	12.0%*	14.0%*
Slab effective mass	0%	1.1%	0%	0.5%	0%	0.3%	0%	0.2%	0%	0.5%
Model approximations	-	-	-	-	-	-	-	-	-	-
Source spectrum	4.8%	4.8%	2.0%*	2.0%*	1.5%	1.5%	0.4%	0.4%	15.4%	15.4%
Monte Carlo statistics	2.6%	6.6%	2.8%	4.6%	2.0%	4.2%	8.0%	6.4%	6.4%	9.2%
TOTAL	14.1%	63.4%	12.0%	32.0%	10.4%	20.7%	12.7%	15.6%	22.1%	46.5%

* Estimated value

Note : all uncertainties are quoted at the 2 s.d. level

Table 19

Uncertainties on detector cross-sections

Group	Lower Energy (MeV)	Sulphur	Rhodium	Gold
1	4.4	7%	5%	7%
2	2.6	12%	4%	7%
3	1.35	12%	4%	7%
4	0.71	12%	7%	7%
5	0.58	-	4%	7%
6	0.41	-	9%	6%
7	0.31	-	9%	6%
8	0.26	-	11%	6%
9	6.2E-2	-	11%	6%
10	3.0E-2	-	-	6%
11	1.5E-2	-	-	6%
12	1.6E-3	-	-	5%
13	2.1E-4	-	-	5%
14	1.1E-5	-	-	5%
15	5.0E-6	-	-	4%
16	5.5E-7	-	-	4%

Table 20

Iron 88 single material benchmark

Comparison of JEF2 predictions of reaction rates using different methods of evaluating the in-group Fe56 cross-section.
Shielded/Dilute

Position	Shield thickness (cm)	S32(n,p)P32	Uncertainty (2 sd)	In115(n,n')In115m	Uncertainty (2 sd)	Rh103(n,n')Rh103m	Uncertainty (2 sd)	Au197(n,g)Au198/Cd	Uncertainty (2 sd)
A2	0.00	0.98	0.04	0.99	0.04	0.99	0.03	1.00	0.10
A3	5.10	1.00	0.04	1.00	0.04	1.04	0.04	0.97	0.06
A4	10.22	1.00	0.04	1.02	0.04	1.04	0.03	1.02	0.08
A5	15.34	1.01	0.04	1.06	0.04	1.08	0.03	1.05	0.07
A6	20.44	1.00	0.05	1.10	0.05	1.13	0.03	1.06	0.08
A7	25.64	1.03	0.05	1.16	0.06	1.15	0.04	1.07	0.07
A8	30.79	1.04	0.05	1.22	0.07	1.25	0.03	1.08	0.06
A9	35.99	1.05	0.05	1.38	0.19	1.30	0.04	1.08	0.06
A10	41.19	1.07	0.06	1.42	0.12	1.31	0.04	1.07	0.06
A11	46.44	1.11	0.07	1.54	0.11	1.42	0.05	1.20	0.26
A12	51.62	1.14	0.07	1.70	0.15	1.40	0.09	1.41	0.45
A13	56.69	1.19	0.08	1.77	0.13	1.51	0.05	1.14	0.07
A14	61.81	1.13	0.08	1.86	0.19	1.52	0.08	1.22	0.08
A15	66.99	1.08	0.10	2.16	0.29	1.65	0.09	1.17	0.11

The quoted uncertainties (2 s.d.) are due to Monte Carlo stochastic error.

Table 21

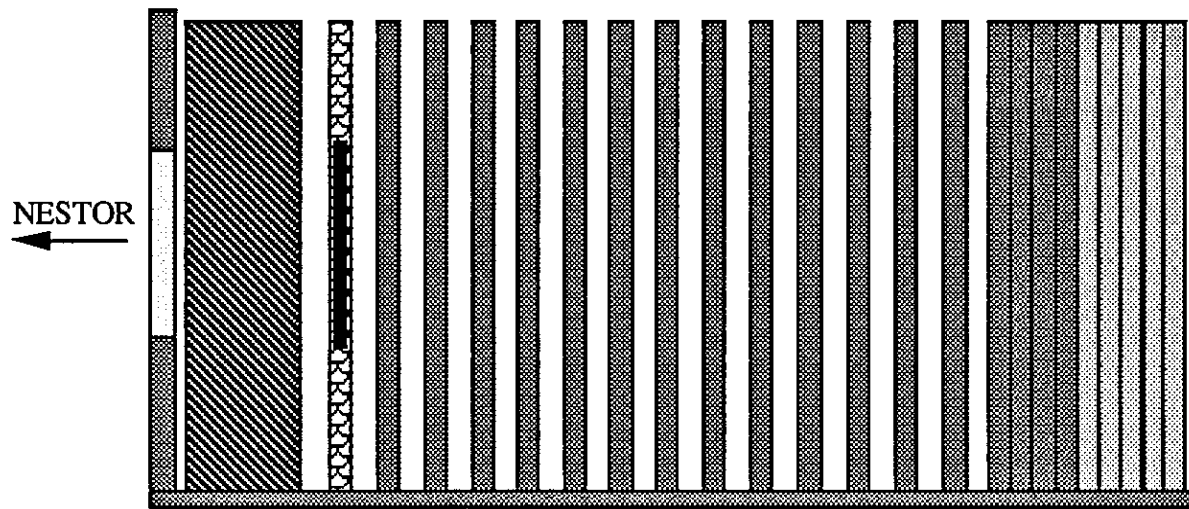
Iron 88 single material benchmark

Comparison of JEF2 predictions of reaction rates using different methods of evaluating the in-group Fe56 cross-section.
Subgroup/Dilute

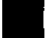





Position	Shield thickness (cm)	S32(n,p)P32	Uncertainty (2 sd)	In115(n,n')In115m	Uncertainty (2 sd)	Rh103(n,n')Rh103m	Uncertainty (2 sd)	Au197(n,g)Au198/Cd	Uncertainty (2 sd)
A2	0.00	0.97	0.04	0.99	0.04	0.99	0.03	1.01	0.10
A3	5.10	1.00	0.04	0.97	0.04	0.99	0.03	0.97	0.06
A4	10.22	1.01	0.04	1.02	0.05	1.01	0.03	1.01	0.06
A5	15.34	1.03	0.04	1.05	0.05	1.03	0.03	1.03	0.07
A6	20.44	1.03	0.05	1.10	0.06	1.08	0.03	1.02	0.07
A7	25.64	1.05	0.05	1.15	0.06	1.11	0.04	0.99	0.08
A8	30.79	1.07	0.05	1.21	0.08	1.21	0.04	1.05	0.09
A9	35.99	1.08	0.06	1.22	0.08	1.23	0.04	0.99	0.07
A10	41.19	1.08	0.06	1.34	0.10	1.25	0.04	1.00	0.06
A11	46.44	1.12	0.06	1.50	0.11	1.37	0.05	0.98	0.06
A12	51.62	1.15	0.07	1.70	0.14	1.39	0.09	1.00	0.07
A13	56.69	1.20	0.08	1.81	0.14	1.56	0.06	1.03	0.06
A14	61.81	1.24	0.09	1.90	0.19	1.53	0.09	1.13	0.07
A15	66.99	1.31	0.17	2.23	0.30	1.62	0.09	1.16	0.12

The quoted uncertainties (2 s.d.) are due to Monte Carlo stochastic error.

Figure 1 Schematic side elevation of the shield in the iron 88
single material benchmark experiment



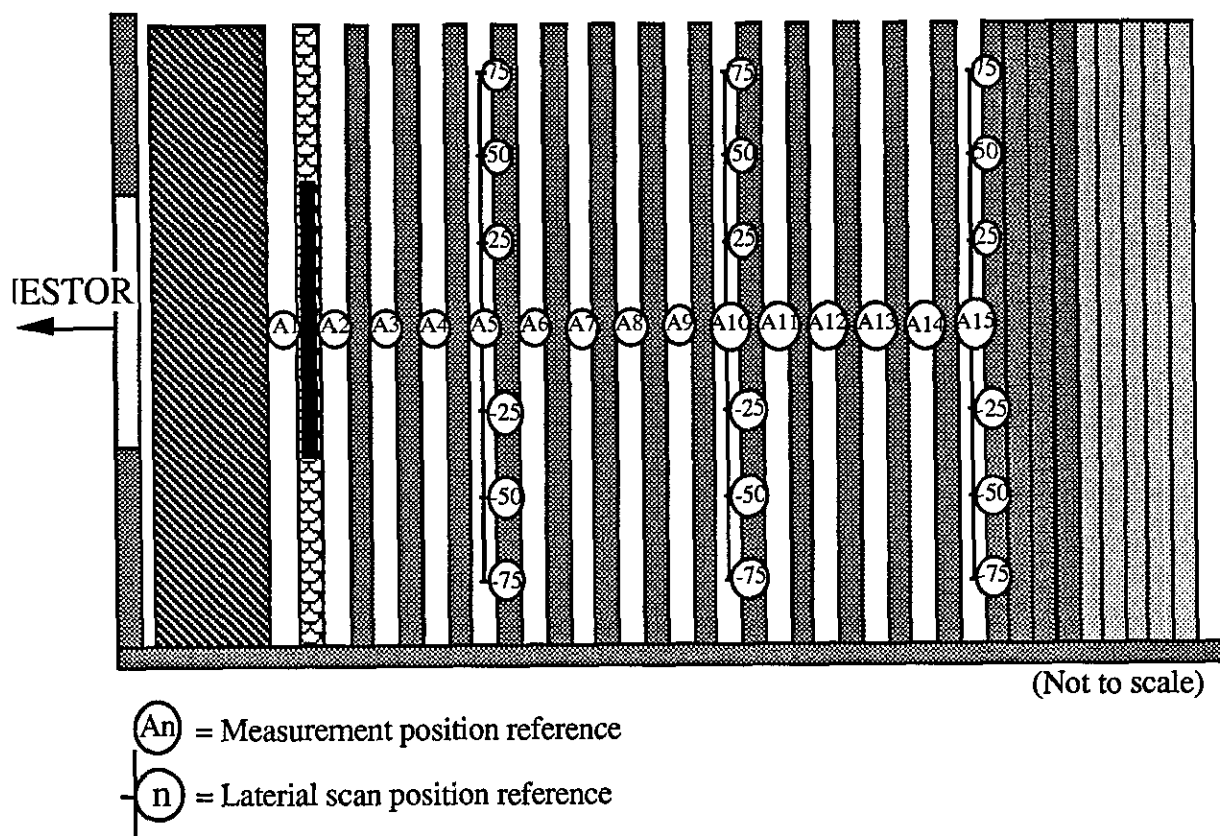
KEY

-  Fuel
-  Mild Steel
-  Stainless Steel
-  Fission Plate
-  Graphite
-  Aluminium

All components are 182.9cm wide by 191.0cm high

Not To Scale

Figure 2 Measurement locations for the iron 88 single material benchmark experiment



Penetration measurements are located on the nuclear centre line as defined below

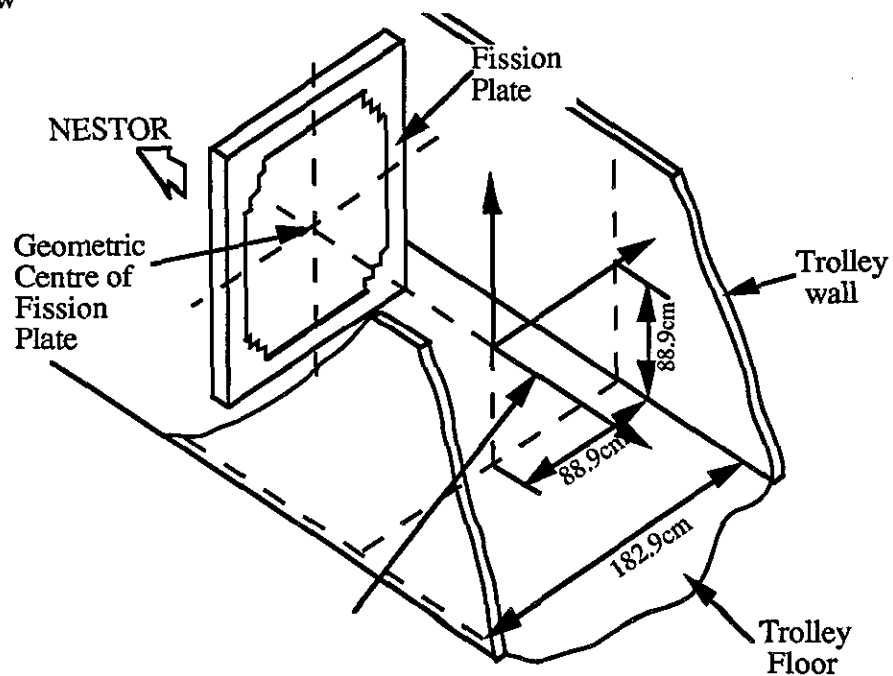


Figure 3 Schematic diagram of fission plate

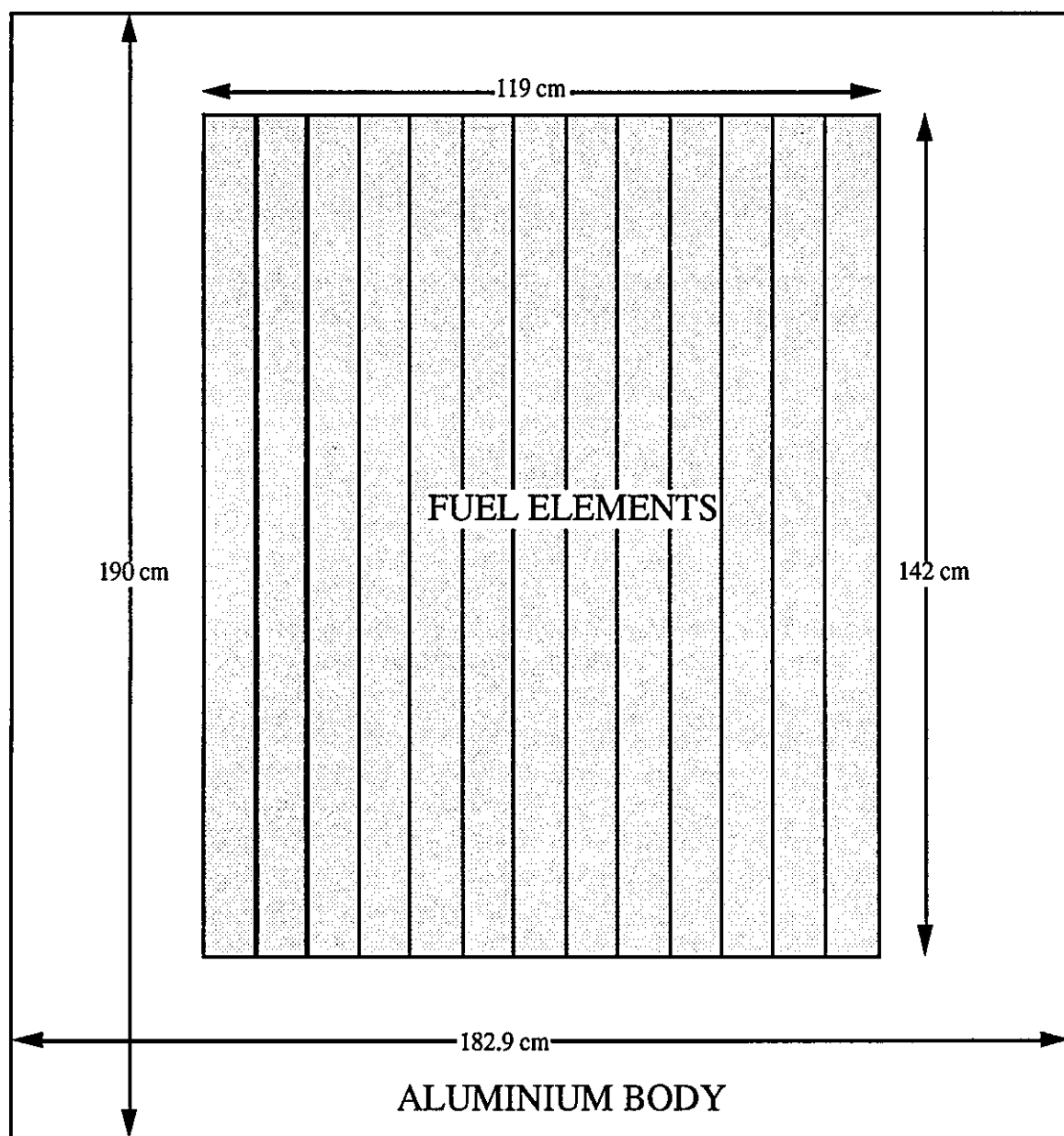
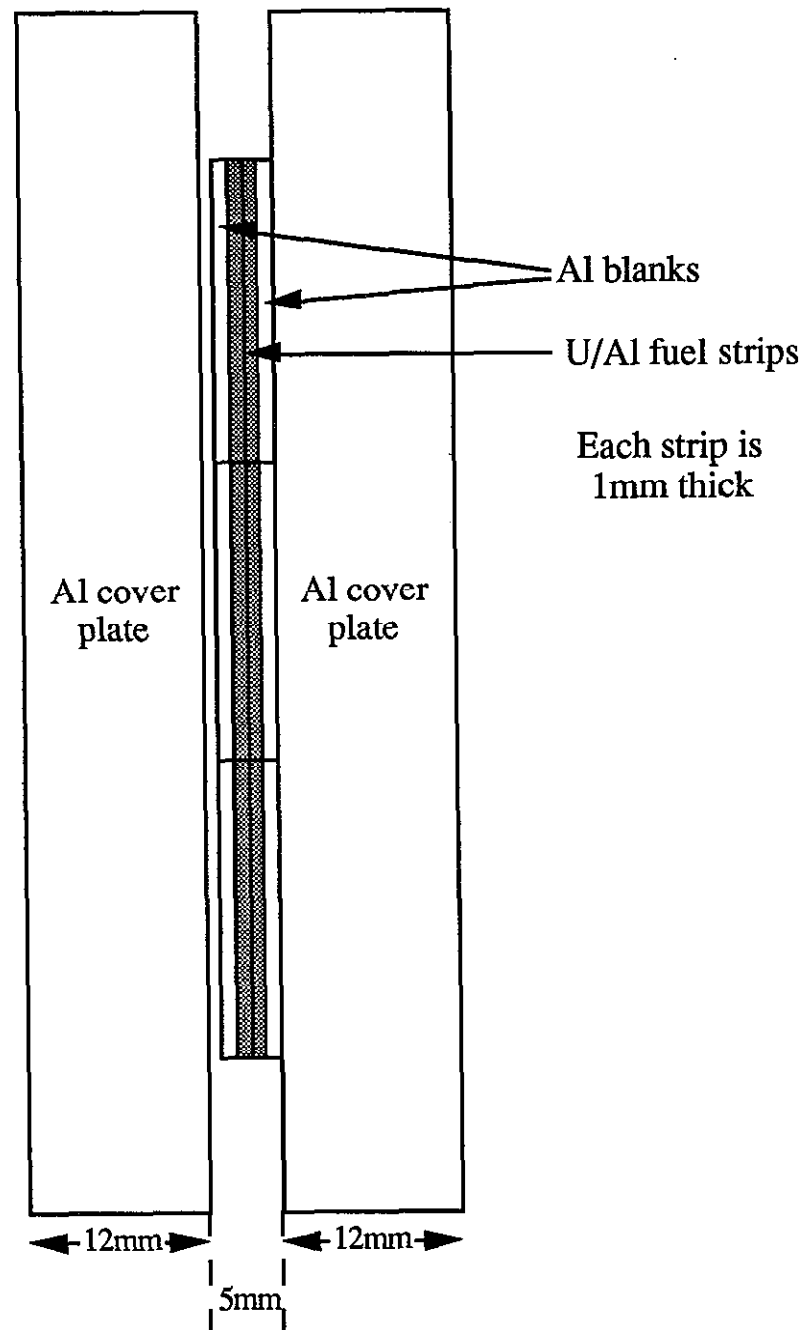


Figure 4 Diagram of fuel element



14090502

Figure 5 Disposition of fuel in fission plate

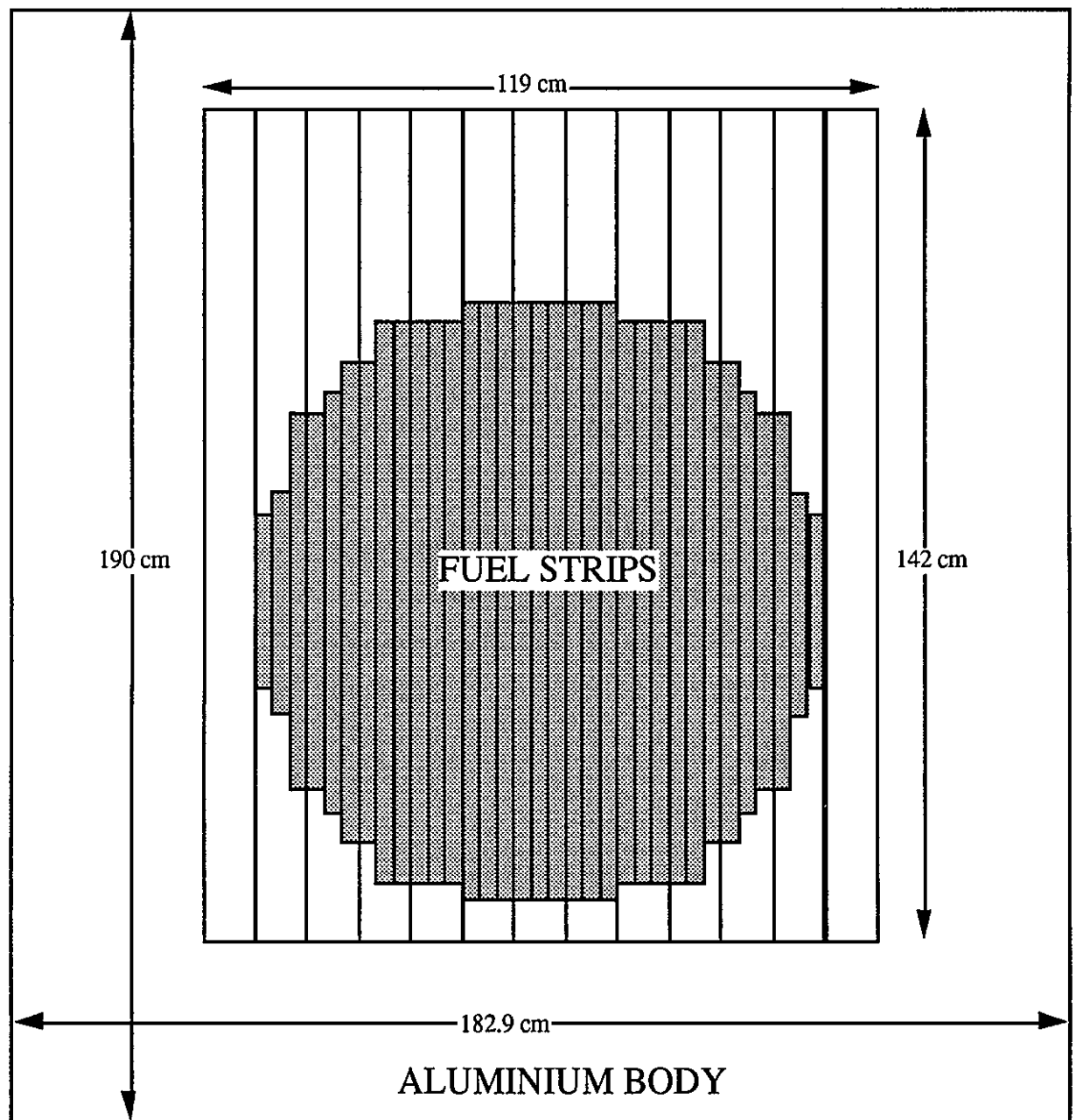
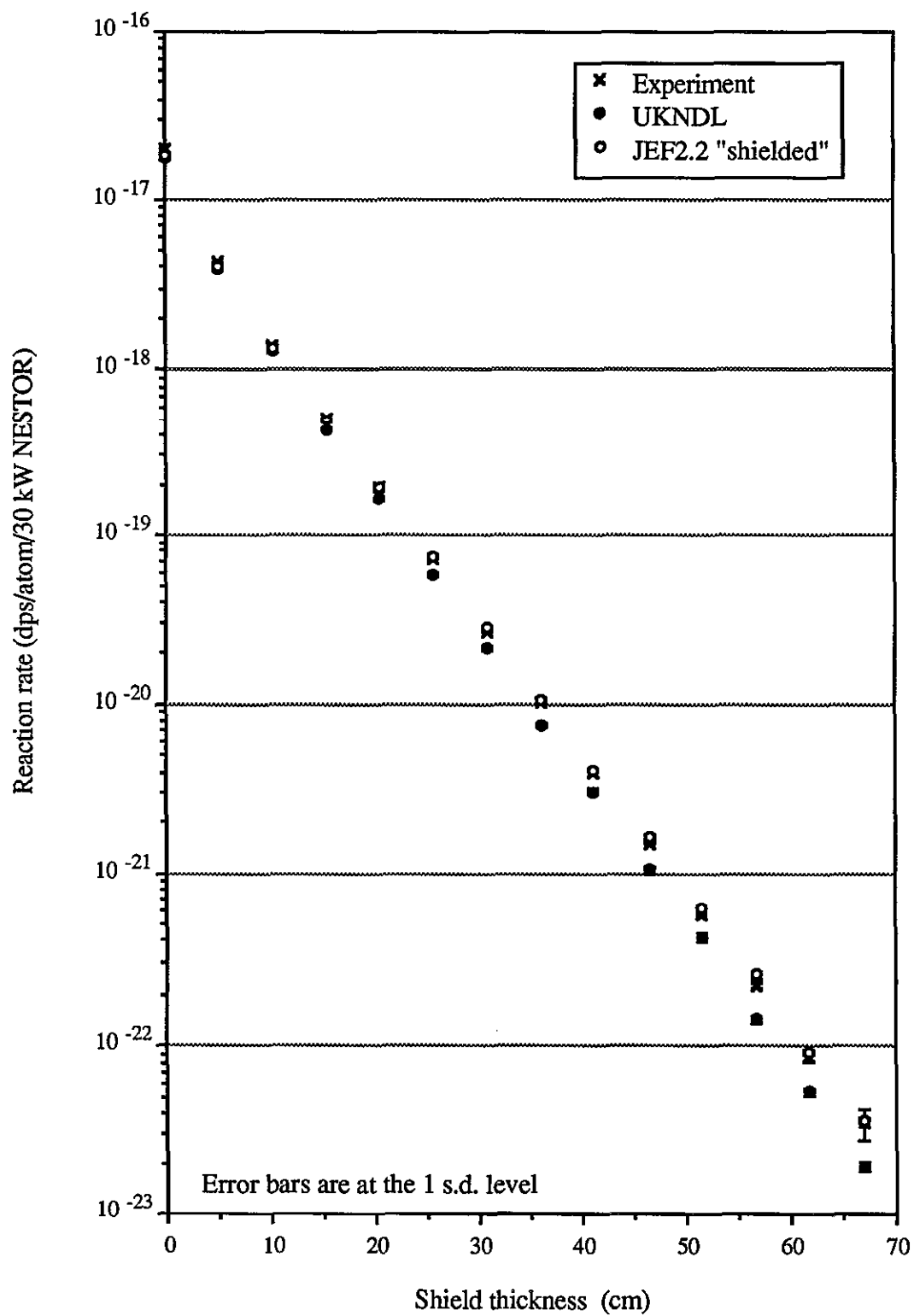
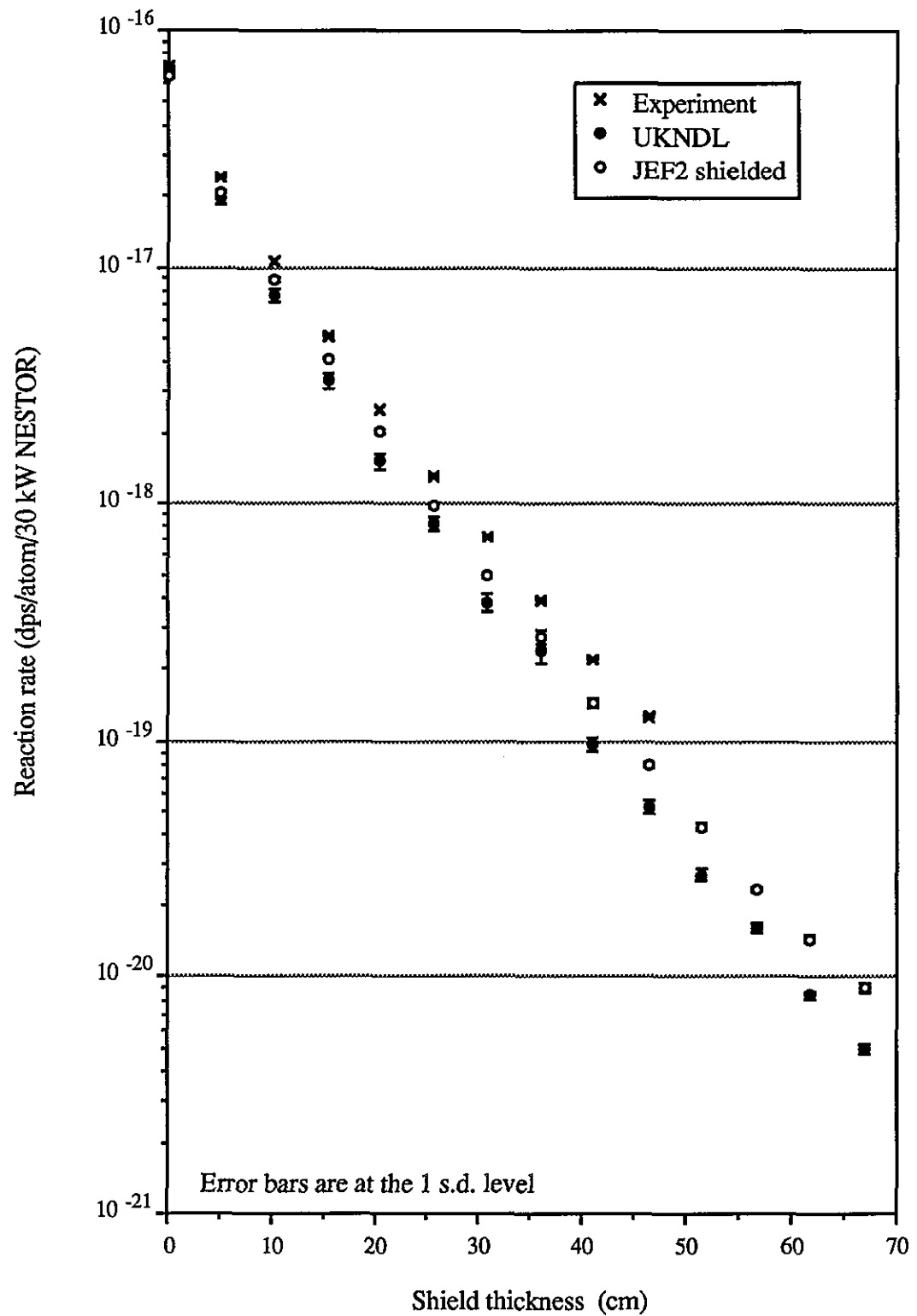


Figure 6 Iron 88 single material benchmark experiment. Predicted and measured S32(n,p)P32 reaction rates along central axis.



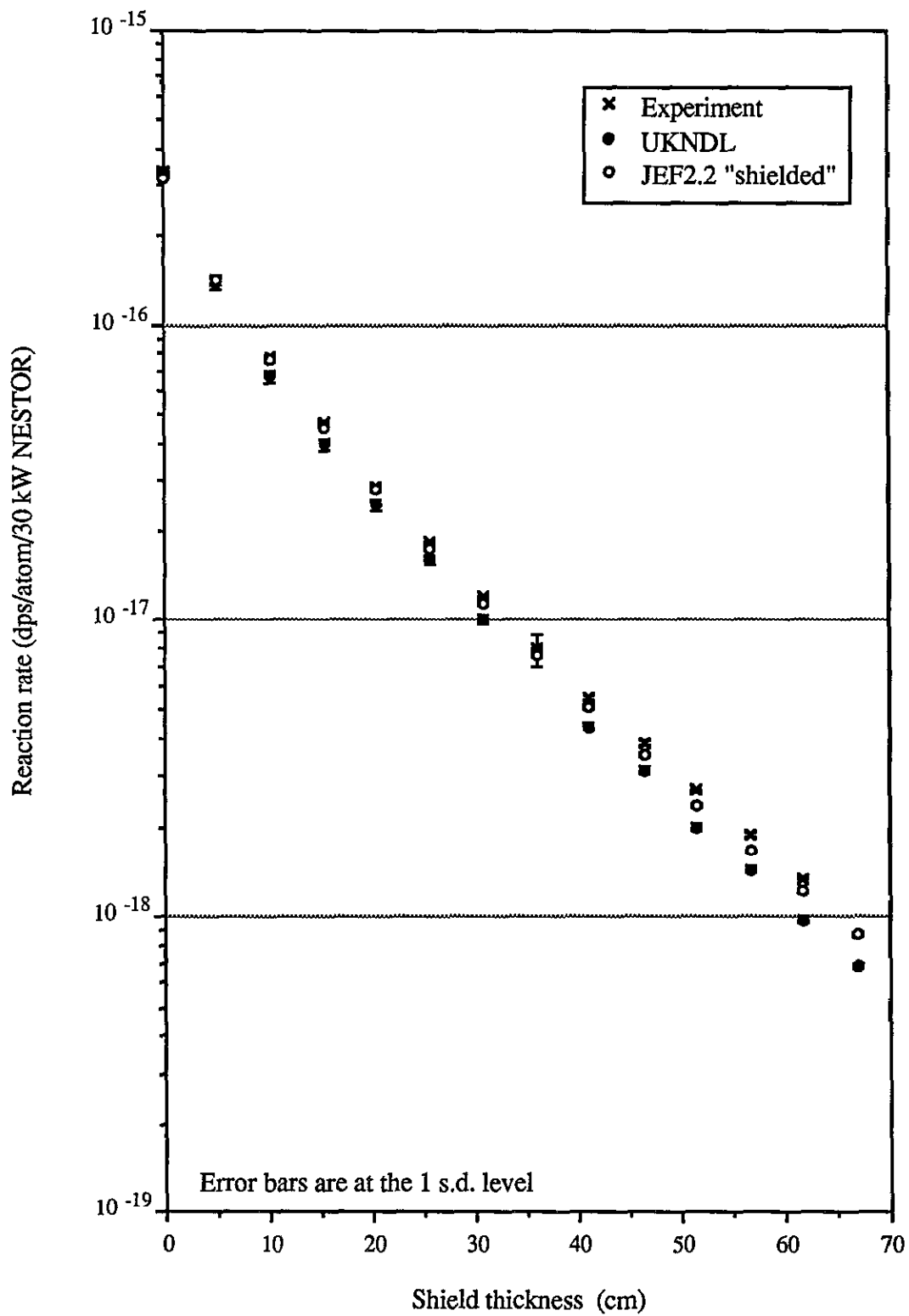
14090504

Figure 7 Iron 88 single material benchmark experiment. Predicted and measured $\text{In115}(n,n')\text{In115m}$ reaction rates along central axis.



14090505

Figure 8 Iron 88 single material benchmark experiment. Predicted and measured Rh103(n,n')Rh103m reaction rates along central axis.



14090506

Figure 9 Iron 88 single material benchmark experiment. Predicted and measured Au197(n, γ)Au198/Cd reaction rates along central axis.

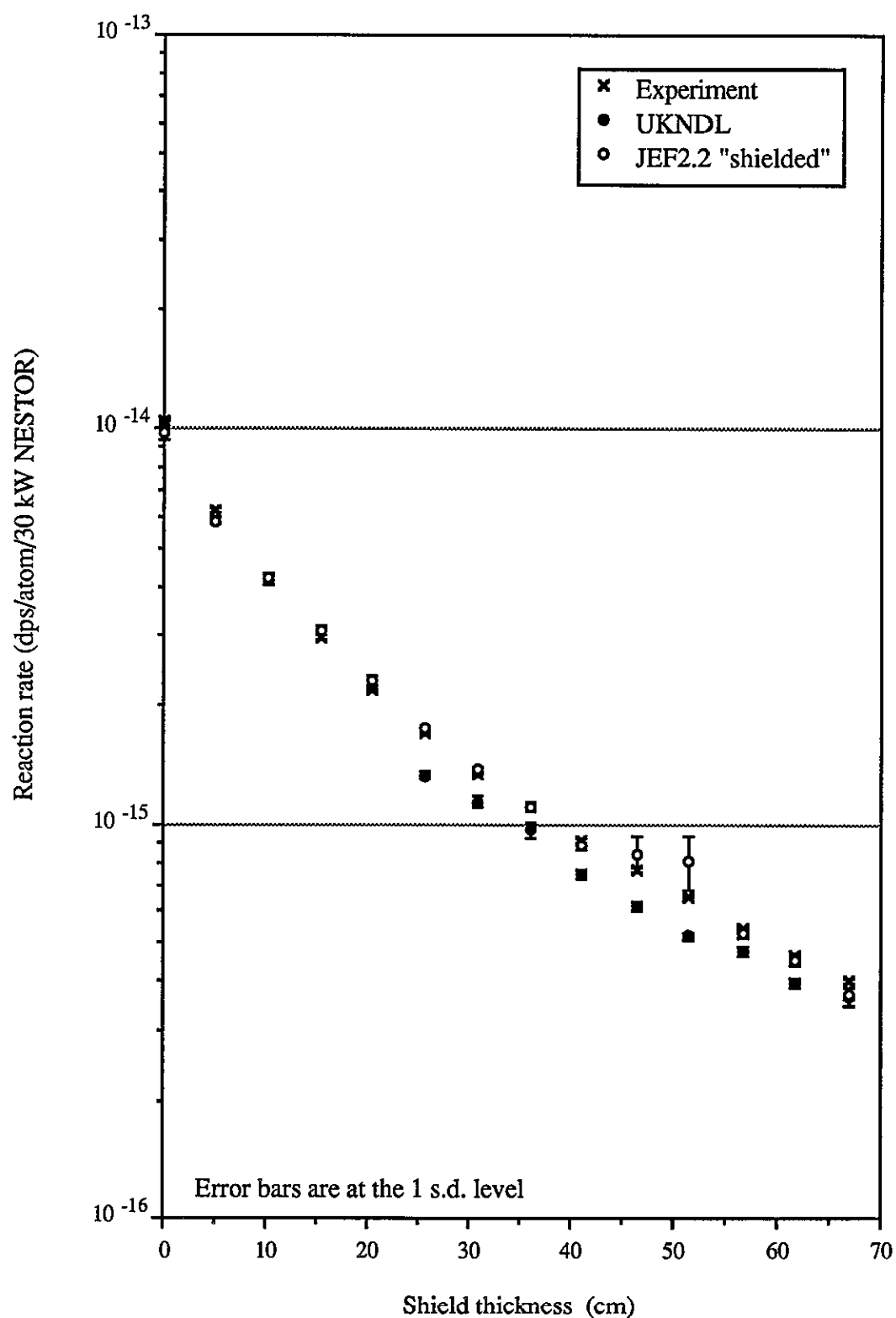


Figure 10 Iron 88 single material benchmark experiment. Predicted and measured $\text{Al}^{27}(\text{n},\alpha)\text{Na}^{24}$ reaction rates along central axis.

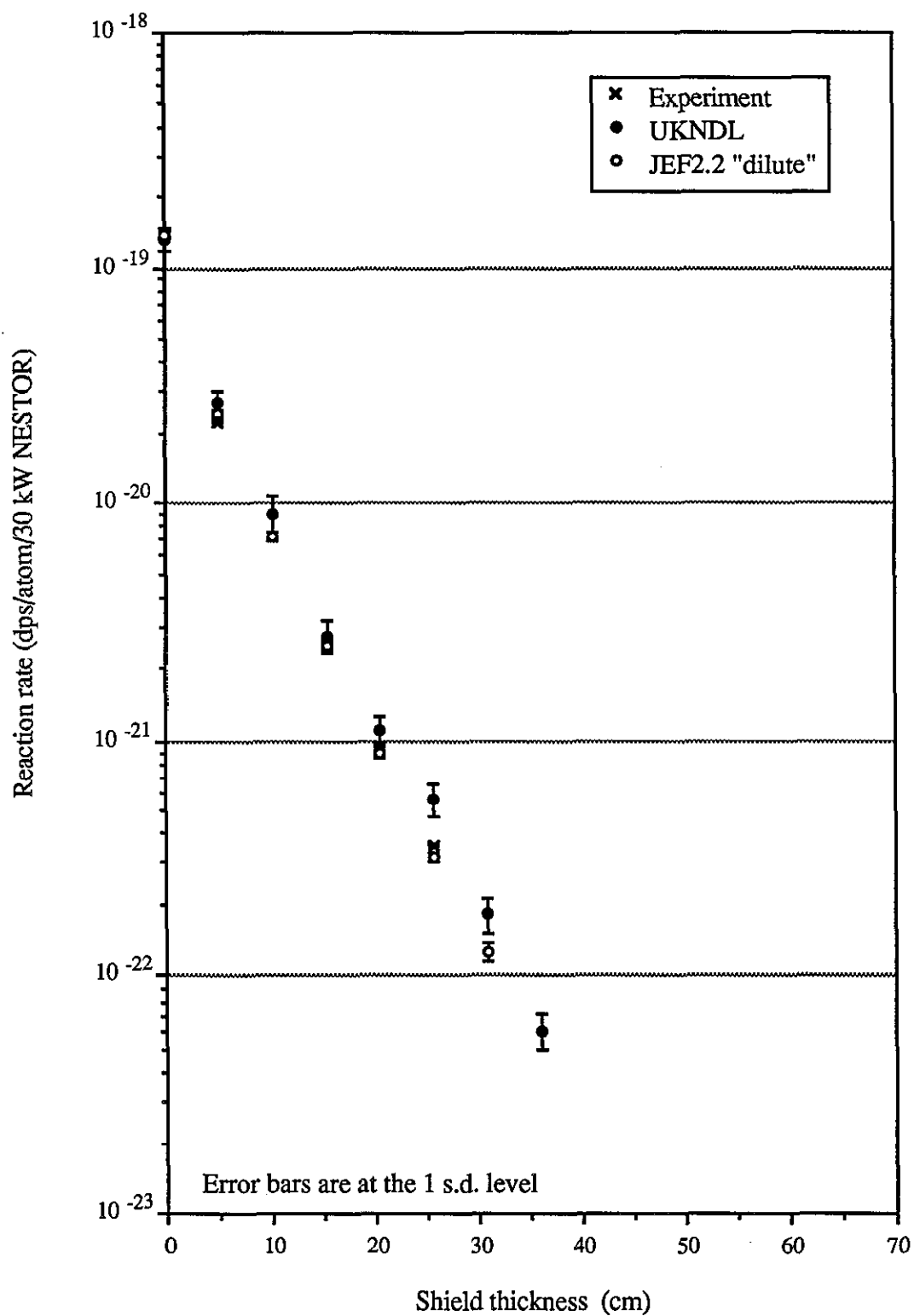


Figure 11 Iron 88 single material benchmark experiment. C/M values for S32(n,p)P32 detector along central axis.

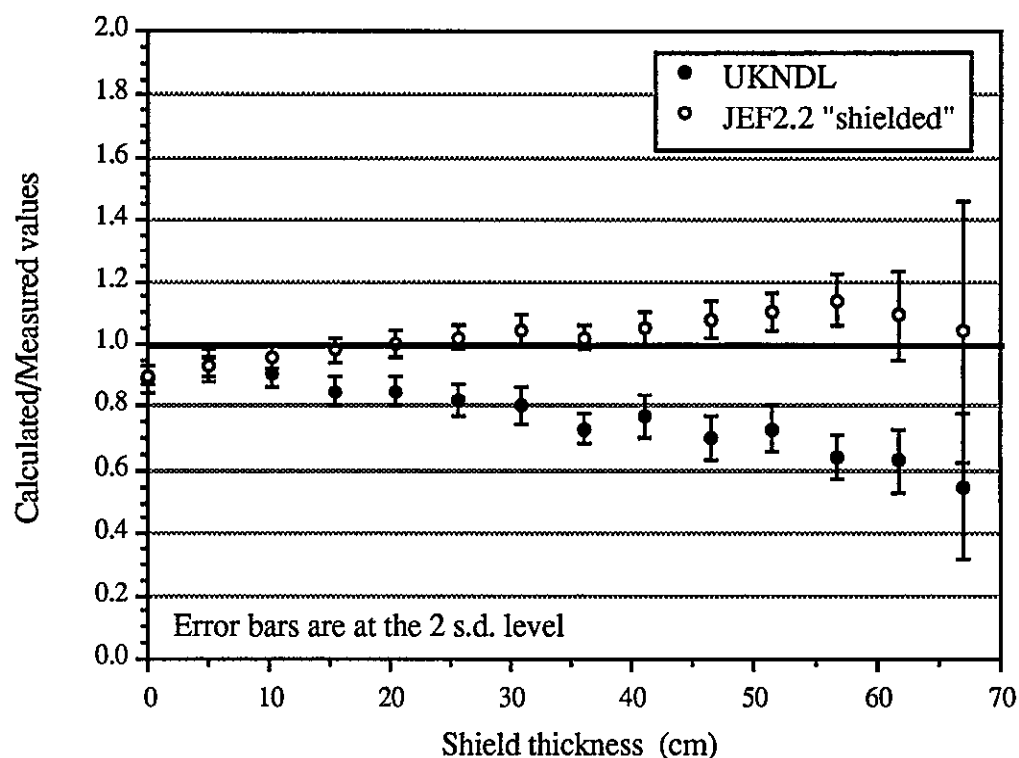


Figure 12 Iron 88 single material benchmark experiment. C/M values for In115(n,n')In115m detector along central axis.

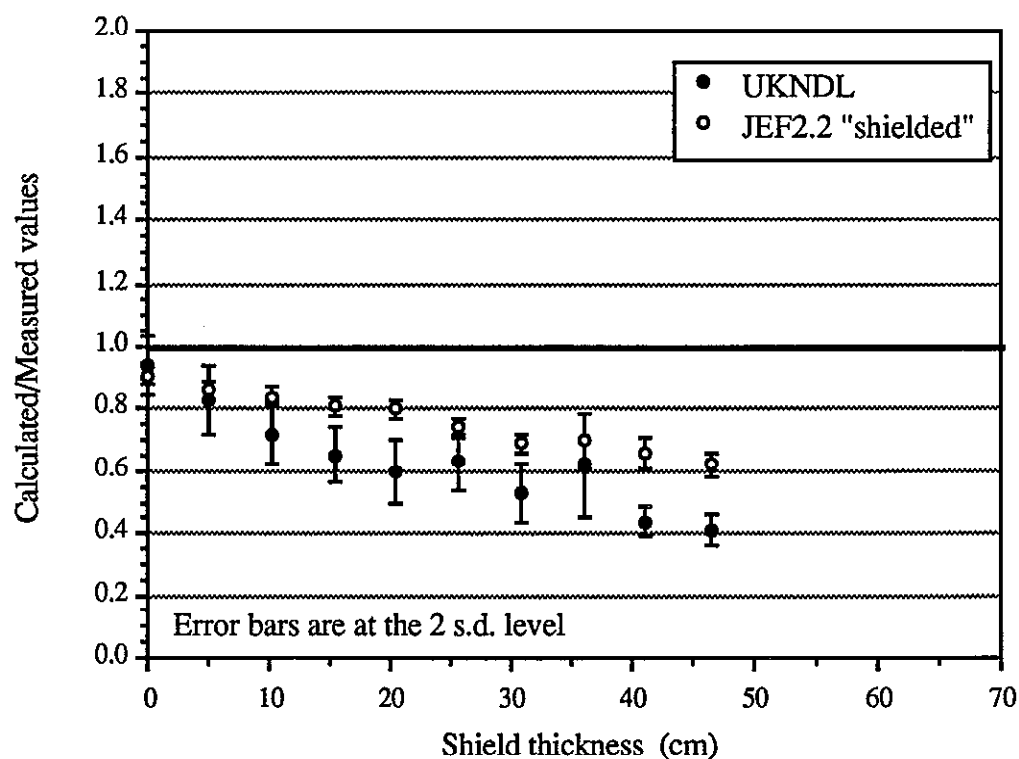


Figure 13 Iron 88 single material benchmark experiment. C/M values for Rh103(n,n')Rh103m detector along central axis.

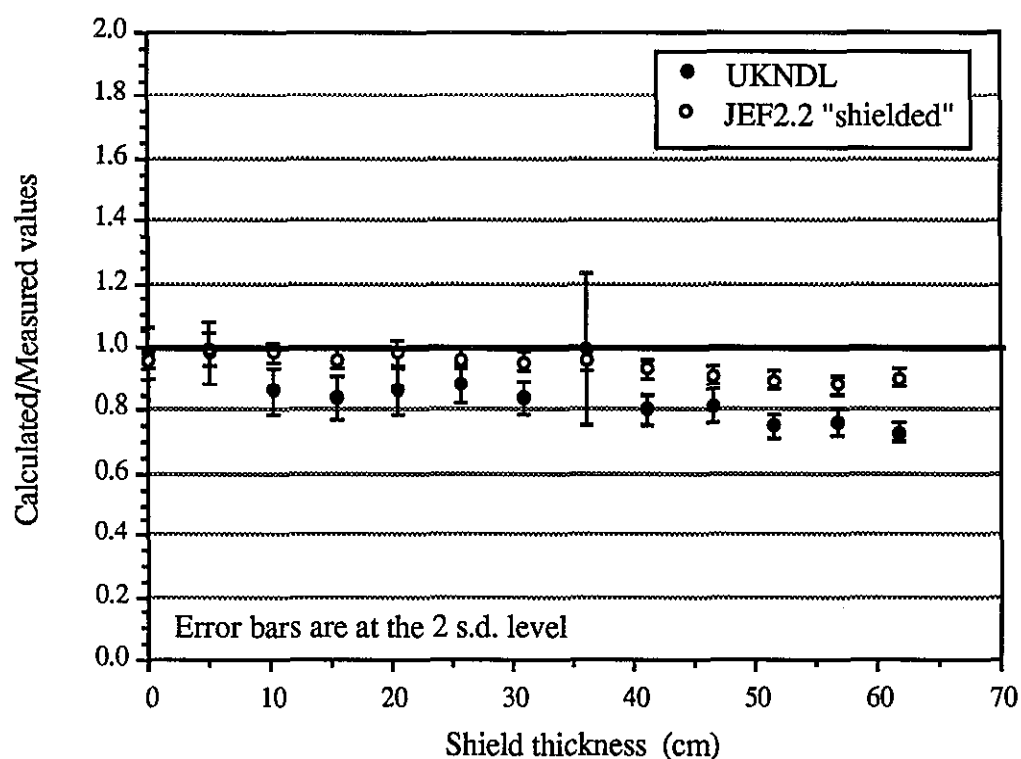
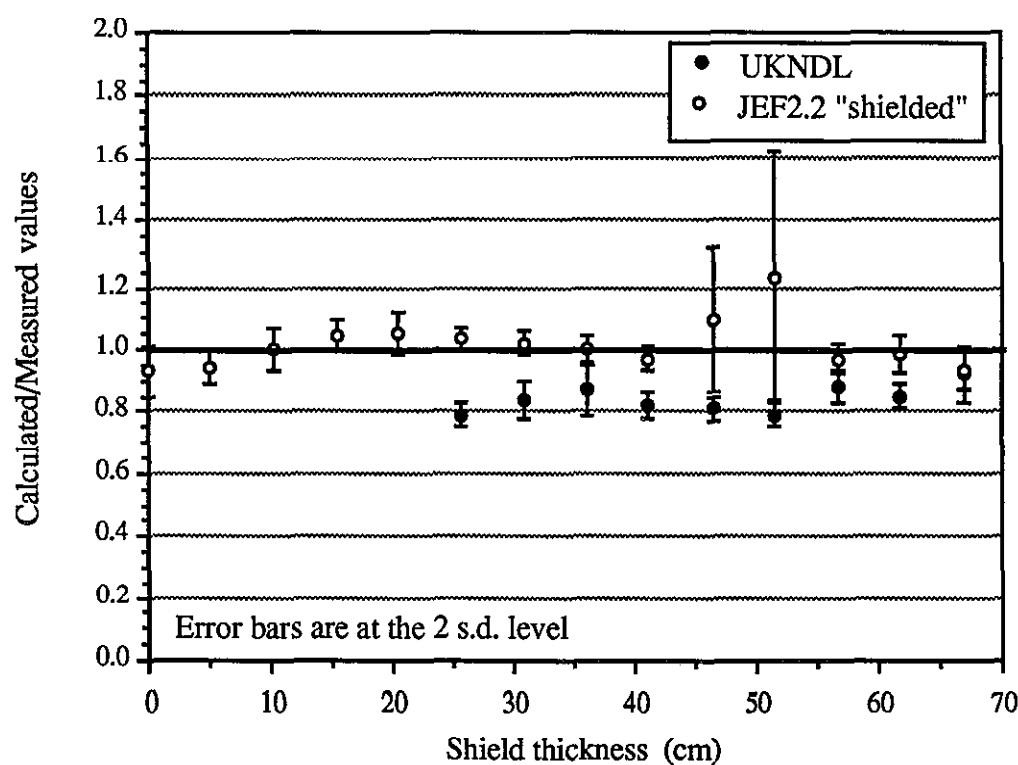


Figure 14 Iron 88 single material benchmark experiment. C/M values for Au197(n, γ)Au198/Cd detector along central axis.



14090510

Figure 15 Iron 88 single material benchmark experiment. C/M values for Al27(n, α)Na24 detector along central axis.

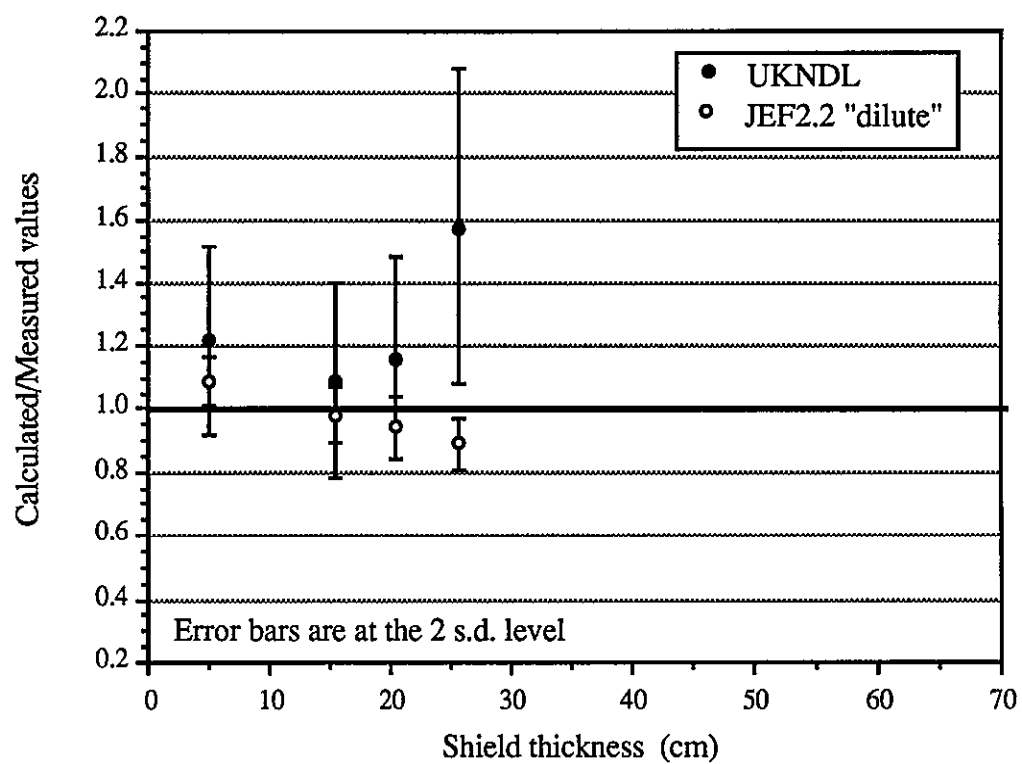


Figure 16 Sensitivity of the S32(n,p)P32 reaction rate after 67 cm of mild steel to the Fe56 cross-sections.

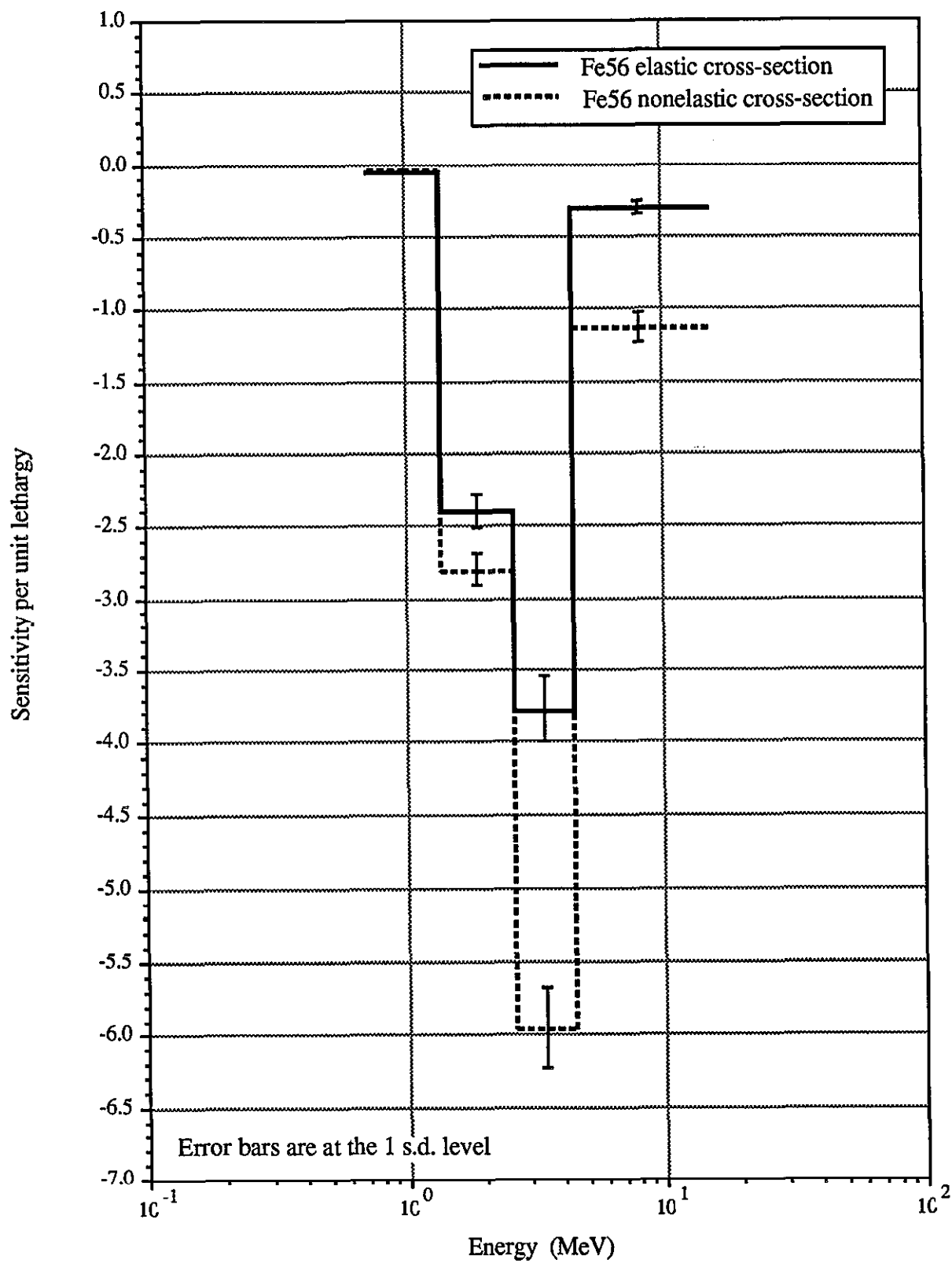


Figure 17 Sensitivity of the $\text{In115}(n,n')\text{In115m}$ reaction rate after 67 cm of mild steel to the Fe56 cross-sections.

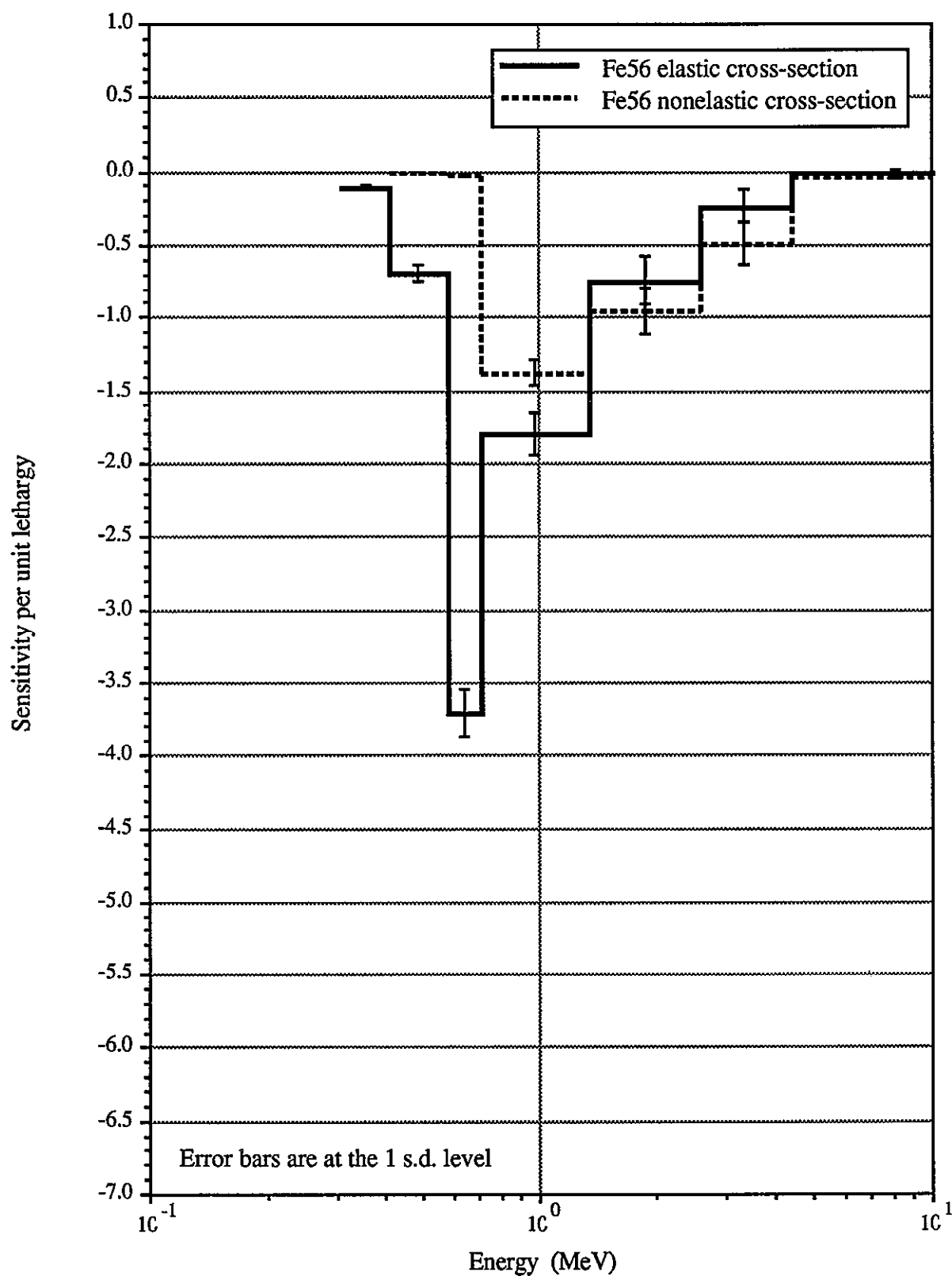


Figure 18 Sensitivity of the Rh103(n,n')Rh103m reaction rate after 67 cm of mild steel to the Fe56 cross-sections.

